Traffic Flow Models and Their Numerical Solutions

By

Wenlong Jin

B.S. (University of Science and Technology of China, Anhui, China) 1998

THESIS

Submitted in partial satisfaction of the requirements for the degree of

MASTER OF SCHIENCE

in

APPLIED MATHEMATICS

in the

OFFICE OF GRADUATE STUDIES

of the

UNIVERSITY OF CALIFORNIA

DAVIS

Approved:

Dr. Michael Zhang

Dr. Elbridge Gerry Puckett

Dr. Albert Fannjiang

Committee in Charge

2000

Contents

ACKNOWLEDGEMENTS

This thesis is written as a summary of my work in last two years at UC Davis. At the moment when I finish my thesis, I want to express my sincere appreciation to those who have enthusiastically taught and helped me all the time.

First, many thanks go to my advisor, Dr. Michael Zhang. About one year ago, he introduced me to the area of transportation studies. Since then, I've worked on several projects on traffic flow models and ramp metering methods, and this thesis is nothing more than a combination of those projects. During the time when I work with him, he gave me many helpful suggestions on how to carry out researches and how to write down my ideas.

I must also thank Dr. Elbridge Gerry Puckett, my academic advisor and the committee member of my thesis. He spent a great deal of time in answering all kinds of questions that I concern. He carefully read and revised my thesis. His suggestions on writing and comments on research will continue to influence my research in the future. He also introduced me to his colleagues, including Dr. Randall J. LeVeque and Dr. Phillip Colella, to whom I also owe my thanks for their help.

To Dr. Albert Fannjiang, I gave my thanks for his important comments on my thesis and serving in the committee of this thesis.

I'm grateful to Dr. Zhaojun Bai who gave me many good suggestions.

I also want to thank my former classmate, Sheng Lu and my former roommate, Dr. John Hong, for sharing their ideas with me.

I should like to take this opportunity to thank Bill Broadley and Zach Johnson, the computer system administrators, whose support is important for so many computations in my projects.

Finally I want to thank my girlfriend, Ling, my parents, Jiasheng and Jiefang, my sister, Xiulian and my brothers, Zhongsheng, Wenhu, and Wenbin for being constant source of encouragement and support.

Chapter 1

Introduction

1.1 Motivation and Problem Definition

Traffic networks – consisting of highways, streets, and other kinds of roadways – provide convenient and economical conveyance of passengers and goods. The basic activity in transportation is a trip, defined by its origin/destination, departure time/arrival time and travel route. A myriad of trips interact on the network to produce an intricate pattern of traffic flows. Since traffic conditions in many major metropolitan areas are becoming increasingly congested, affecting the operational efficiency of whole networks as well as the travel cost of each trip, traffic flow models are becoming more important in traffic engineering and the transportation policy making process. For example, well-developed traffic models are used in developing advanced ramp metering methods as well as in determining dynamic traffic assignment (JWL & Zhang, 2000a).

There have been two approaches in mathematical modeling of traffic flow. One approach, from a microscopic view, studies individual movements of vehicles and interactions between vehicle pairs. This approach considers driving behavior and vehicle pair dynamics. But the size of the problem in a microscopic model becomes mathematically intractable when a considerable volume of traffic flow is considered. One example of the microscopic approach is the GM family of car-following models developed in the 1960's (e.g., Gazis et al., 1961). The other approach studies the macroscopic features of traffic flows such as flow rate q, traffic density ρ and travel speed v. The basic relationship between the three variables is: $q = \rho v$. Macroscopic models are more suitable for modeling traffic flow in complex networks since less supporting data and computation are needed.

In this thesis macroscopic traffic flow models are studied both theoretically and numerically. Traffic flows are classified according to traffic conditions, roadway conditions and traffic network structure. Traffic flows are in equilibrium when the travel speed of these flows is uniquely determined as a function of traffic density, otherwise they are in non-equilibrium. Traffic flows are considered inhomogeneous when the roadway has different parameters at different locations. Link flows are flows on road links, and network flows are traffic flows on networks of roadways. Network flows differ from link flows in that vehicles in the former have different characteristics which affect traffic dynamics, such as the origins or destinations.

Different types of traffic flow are described by different models. For equilibrium link flow, the celebrated LWR model was developed by Lighthill and Whitham (1955) and Richards (1956). The LWR model has been solved for the homogeneous roadway rigorously. There have been empirical solutions to the inhomogeneous LWR model. In this work a rigorous procedure to solve the inhomogeneous LWR model is developed. (JWL & Zhang, 2000b). The LWR model is a first-order model in the sense of PDE system order. In this thesis we also discuss the PW model (Payne, 1971; Whitham, 1974) and Zhang's model (1998, 1999a) for non-equilibrium link flow. Finally we introduce a multi-commodity model when traffic flow is disaggregated by origins, destinations or departure times.

All the models we consider are based on conservation of traffic flow, i.e., the increment of vehicles in a section is equal to the difference between upstream influx and downstream out-flux in unit time. Mathematically, every model except the multi-commodity model, which is a discrete model, can be written as a continuous system of hyperbolic conservation laws. Solutions to the Riemann problem for all the continuous models are studied analytically, and all the models including the multi-commodity model are solved numerically with Godunov type of methods.

1.2 Background and Research Overview

1.2.1 Traffic Flow Models

In what follows the term "traffic flow model" means a macroscopic traffic flow model. Many continuum traffic flow models can be described by a system of hyperbolic PDEs. The first of these models was the LWR model. This model relies on the assumption that there exists an equilibrium speed-density relationship $v = v_*(\rho)$. Like other dynamic continuum flow models the LWR model is based on the mass conservation, i.e., traffic conservation, and is described by a first-order, nonlinear PDE:

$$\rho_t + f(\rho)_x = 0, \tag{1.1}$$

in which $f(\rho) = \rho v_*(\rho)$ is the traffic flow rate. Equation (1.1) is in conservation form. It is also called a kinematic wave model since it shows wave properties analogous to those of gases. There are many numerical methods to solve the LWR model. One approach is to solve the Riemann problem and apply a Godunov method for this model. Both solutions to the Riemann problem and the Godunov method are well-developed for hyperbolic conservation laws (Smoller, 1983). Another approach is to use the demand and supply functions (Lebacque, 1996; Daganzo, 1995), which turns out to be variants of Godunov's method.

The PW model, derived based on microscopic car-following models, discards the equilibrium assumption. It is a second-order system of hyperbolic conservation laws with a source term:

$$\rho_t + (\rho v)_x = 0, \tag{1.2}$$

$$v_t + v v_x + \frac{c_0^2}{\rho}\rho_x = \frac{v_*(\rho) - v}{\tau}, \tag{1.3}$$

in which the constant c_0 is the traffic sound speed and τ is the relaxation time. Equation (1.2) is the continuity equation, and (1.3) is the momentum equation. The PW model relates to driver behavior models better than the LWR model because it accounts for drivers' anticipation and inertia. However it's been shown that the LWR model is an asymptotic approximation of the PW model (Schochet, 1988). The PW model better captures non-equilibrium wave phenomena in traffic flow. Another property of the PW model is that it is unstable under certain situations. Since there are no known analytical solutions to the PW model, we use numerical methods to solve it in this research. All of these methods are developed from Godunov's method.

Also based on microscopic models, Zhang (1998) developed a new non-equilibrium traffic flow theory :

$$\rho_t + (\rho v)_x = 0, \tag{1.4}$$

$$v_t + v v_x + \frac{(\rho v_*'(\rho))^2}{\rho}\rho_x = \frac{v_*(\rho) - v}{\tau}. \tag{1.5}$$

In the momentum equation (1.5), a varying sound speed $c = \rho v_*'(\rho)$ has been introduced. It has been shown that this new model avoids "wrong-way travel" which is exhibited in the PW model (Zhang, 1998), and the model is always stable. Wave solutions to this model were discussed in (Zhang, 1999a), and finite difference approximations were studied in (Zhang, 2000a). In this research we perform the numerical simulations of this model.

For a roadway with inhomogeneities such as a change in number of lanes, curvature and slopes, the LWR model can still be used, but the equilibrium speed-density relationship varies with location. By introducing an inhomogeneity function $a(x)$ which is a profile of the roadway at the location x, we can write the inhomogeneous LWR model as

$$\rho_t + f(a,\rho)_x = 0. \tag{1.6}$$

Here the traffic flow rate $f(a,\rho)$ is a function of the inhomogeneity $a(x)$. By writing

$$a_t = 0, \tag{1.7}$$

the inhomogeneous LWR model is a non-strictly hyperbolic system. There have been empirical methods to solve the inhomogeneous LWR model (Lebacque, 1995; Daganzo, 1995a). In this research, we develop a rigorous procedure to solve the LWR model based on the work by Isaacson et al. (1992) and Lin et al. (1995). We find the solutions that are consistent with those given by Lebacque. However, our method can be extended to solve higher-order inhomogeneous models while those of Lebacque and Daganzo cannot.

Multi-commodity models are discussed in (Daganzo, 1994 and 1995; Jayakrishnan, 1991; Vaughan et al., 1984). In these models traffic flow is disaggregated by origins, destinations or departure times. All of these models are based on traffic conservation. A First-In-First-Out (FIFO) discipline is assumed in all of these multi-commodity models. The model studied by Vaughan et al. is a continuous model. The models studied by Jayakrishnan and Daganzo are discrete models. In these two discrete models vehicles that are close to each other (in the sense of location or time) and have the same origin or destination or some other common characteristics are combined as a macroparticle. The macroparticles in a zone are ordered by time or location. Macroparticles are moved according to traffic conditions, which are solved with a link flow model. In the thesis, we introduce a new multi-commodity model that is more efficient in moving macroparticles.

1.2.2 Hyperbolic Systems of Conservation Laws and Godunov Methods

A system of hyperbolic conservation laws (Smoller, 1983) takes the following form:

$$u_t + f(u)_x = 0, \tag{1.8}$$

where $u = (u_1, \cdots, u_n) \in \mathbb{R}^n, n \geq 1$, and $(x, t) \in \mathbb{R} \times \mathbb{R}_+$. The n eigenvalues of the differential of $f(u)$, $Df(u)$, are denoted as $\lambda_1, \cdots, \lambda_n$. The solutions related to i-th eigenvalue are called i-family wave solutions. If the eigenvalues are distinct, the system (1.8) is a strictly hyperbolic system. To solve (1.8), initial and boundary conditions are needed. The Riemann problem is to solve (1.8) with the following jump initial condition:

$$u(x, t = 0) = \begin{cases} u_l, & x < 0 \\ u_r, & x > 0 \end{cases}, \tag{1.9}$$

where u_l and $u - r$ are constants.

It is well-known that the weak solutions to the Riemann problem exist and are unique for the system (1.8) under the so-called "Lax's entropy condition" (Lax, 1972). The system admits discontinuous solutions, i.e., shock waves, and the wave speed s is determined by Rankine-Hugoniot condition:

$$s[u] = [f(u)], \tag{1.10}$$

where $[u] = u_l - u_r$, and similarly, $[f(u)] = f(u_l) - f(u_r)$. For valid i-family shock wave solutions, the entropy inequalities hold, i.e., $\lambda_i(u_l) > s > \lambda_i(u_r)$. There are continuous solutions $u = u(\xi)$, $\xi = x/t$, which satisfy the ordinary differential equations

$$-\xi u_\xi + f(u)_\xi = 0. \tag{1.11}$$

For most general initial and boundary conditions, there are no analytical solutions to (1.8), hence, one must use numerical methods to solve it. The Godunov method is one of the most efficient numerical methods, which combines solutions to the Riemann problem and conservation laws. In a Godunov method, the space region $[a, b]$ is divided into N grids $x_0 = a, x_1, \cdots, x_{N-1}, x_N = b$; the time scale $[t_0, t_1]$ are partitioned into M time steps $t^0 = t_0, t^1, \cdots, t^{M-1}, t^M = t_1$. The hyperbolic system of conservation laws (1.8) can be approximated by the finite difference equations:

$$\frac{U_i^{j+1} - U_i^j}{\Delta t} + \frac{f(U_{i-1/2}^*) - f(U_{i+1/2}^*)}{\Delta x} = 0, \tag{1.12}$$

where U_i^j is the average of $u(x,t)$ in grid $[x_{i-1/2}, x_{i+1/2}]$ at time step t_j, similarly U_i^{j+1} is the average at time step t_{j+1}; $U_{i-1/2}^*$ is the average of $u(x,t)$ during time interval $[t_j, t_{j+1}]$ at grid boundary $x_{i-1/2}$, similarly $U_{i+1/2}^*$ is the average at boundary $x_{i+1/2}$. The boundary flux $f(U_{i-1/2}^*)$ is calculated by solving a Riemann problem at each cell edge with the following initial conditions:

$$u(x, t^j) = \begin{cases} U_{i-1}^j, & x < x_{i-1/2} \\ U_i^j, & x > x_{i+1/2} \end{cases}.$$

Equations (1.12) says that the increment of u is equal to the difference between both boundary fluxes, which is the general idea of conservation.

In this thesis our second-order models are not exact conservation laws since they have a source term, therefore our methods have been extended to address the effect of source terms.

1.3 Layout of the Thesis

In chapter 2, we study the homogeneous LWR model through theoretical discussions and numerical simulations. This is the first step for us to understand traffic flow models and associated numerical methods. In chapter 3, Godunov-type methods are developed for Zhang's model. The Riemann problem is solved in detail, and computational results are discussed. In chapter 4, the PW model is studied with several different Godunov-type finite difference methods, and the stability of the model is tested. In chapter 5, the Riemann problem for the inhomogeneous LWR model is solved rigorously. In chapter 6, a multi-commodity model based on the LWR model is studied. In chapter 7, possible extensions of this research are discussed.

Chapter 2

The LWR Model and Its Numerical Solutions

The landmark paper by Lighthill and Whitham (1955) set the tone for many researchers' investigations into the theory of traffic flow. Introduced for traffic flows on a single, long, and rather idealized road, the LWR model proposes that their dynamics is described by the following PDE:

$$\rho_t + f(\rho)_x \quad = \quad 0, \tag{2.1}$$

where subscript t means the partial derivative with respect to time t, and subscript x means the partial derivative with respect to location x. In (2.1), the function $f(\rho) = \rho v_*(\rho)$ is called the fundamental diagram of traffic flow, in which $v_*(\rho)$ reflects the equilibrium relationship between travel speed and traffic density. It's generally assumed that $f(\rho)$ is a concave function, i.e., $f_{\rho\rho}(\rho) < 0$. The characteristic wave speed $\lambda(\rho) = f_\rho(\rho) = v_*(\rho) + \rho v_*'(\rho)$. $\lambda(\rho)$ can be positive or negative.

Weak solutions (Smoller, 1983) for (2.1) satisfy the integral form of the conservation law:

$$\frac{\partial}{\partial t}\int_{x_1}^{x_2} \rho(x,t)\mathrm{dx} \quad = \quad f(x_1,t) - f(x_2,t). \tag{2.2}$$

First, we discuss the Riemann problem for (2.1) theoretically and then give the numerical solutions.

2.1 The Riemann problem

We consider the Riemann problem for the LWR model with the following jump initial condition:

$$\rho(x, t=0) = \begin{cases} \rho_l, & x < 0 \\ \rho_r, & x > 0 \end{cases}. \tag{2.3}$$

There are two types of wave solutions to the Riemann problem. The discontinuous solution is a shock wave

$$\rho(x, t>0) = \begin{cases} \rho_l, & x/t < s \\ \rho_r, & x/t > s \end{cases}, \tag{2.4}$$

where s is the shock wave speed. The shock wave speed is determined by the Rankine-Hugoniot jump condition,

$$s = \frac{[f(\rho)]}{[\rho]}. \tag{2.5}$$

The wave speed of a valid shock wave solution has to satisfy the entropy condition:

$$\lambda(\rho_l) > s > \lambda(\rho_r). \tag{2.6}$$

Specifically, for a concave fundamental diagram, a shock wave is a solution to the Riemann problem for (2.1) with initial conditions (2.3) when $\rho_l < \rho_r$; i.e., the upstream traffic density is lower.

When the upstream traffic density is higher, solution to the LWR model with initial data (2.3) is a continuous rarefaction wave. The rarefaction wave is given by $\rho = \rho(\xi), \xi = x/t$, where ρ satisfies the ordinary differential equation

$$-\xi\rho_\xi + f(\rho)_\xi = 0. \tag{2.7}$$

If $\rho(\xi) \neq 0$, we obtain

$$\lambda(\rho(\xi)) = \xi, \tag{2.8}$$

from which we can find $\rho(\xi)$ uniquely. On any characteristic $x/t = \xi$, ρ is constant.

2.2 Computation of boundary fluxes

Given a wave solution to the Riemann problem, we can compute the average ρ^* at $x = 0$ and therefore the flux $f(\rho^*)$ through the boundary. There are the following five cases:

Case 1 When the solution to the Riemann problem is a shock wave with wave speed $s > 0$, $\rho^* = \rho_l$.

Case 2 When the solution to the Riemann problem is a shock wave with wave speed $s \leq 0$, $\rho^* = \rho_r$.

Case 3 When the solution to the Riemann problem is a rarefaction wave, and $\lambda(\rho_l) > 0$, $\rho^* = \rho_l$.

Case 4 When the solution to the Riemann problem is a rarefaction wave, and $\lambda(\rho_r) < 0$, $\rho^* = \rho_r$.

Case 5 When the solution to the Riemann problem is a rarefaction wave, $\lambda(\rho_l) < 0$ and $\lambda(\rho_r) > 0$, ρ^* is the solution of $\lambda(\rho^*) = 0$.

Given initial and boundary conditions, we can use a first-order Godunov method to calculate the traffic conditions. The numerical solutions are given in next section.

2.3 Numerical solutions to the LWR model

In this section, we solve the Riemann problem for (1.8) numerically. We use Newell's equilibrium model,

$$v_*(\rho) \;=\; v_f \left(1 - \exp\{\frac{|c_j|}{v_f}(1 - \rho_j/\rho\}\right) \tag{2.9}$$

Without loss of generality, we set $v_f = 1, c_j = 1, \rho_j = 1$ to obtain

$$v_*(\rho) \;=\; 1 - \exp\left(1 - \frac{1}{\rho}\right) \tag{2.10}$$

The valid range for ρ and v is $0 < \rho, v \leq 1$. The corresponding flow rate, $f_* = \rho v_*$, is a normalized fundamental diagram.

1. Given the initial conditions:

$$\rho(x,0) \;=\; \begin{cases} 0.65 & x \in [0l, 200l] \\ 0.4 & \text{otherwise} \end{cases} \tag{2.11}$$

$$v(x,0) \;=\; v_*(\rho(x,0)), \qquad \forall x \in [0l, 800l] \tag{2.12}$$

   we obtain the solutions shown in **Figure** 2.1,**Figure** 2.2.

2. Given the initial conditions:

$$\rho(x,0) \;=\; \begin{cases} 0.65 & x \in [0l, 200l] \\ 0.9 & \text{otherwise} \end{cases} \tag{2.13}$$

$$v(x,0) \;=\; v_*(\rho(x,0)), \qquad \forall x \in [0l, 800l] \tag{2.14}$$

   we obtain the solutions shown in **Figure** 2.3,**Figure** 2.4.

From these numerical solutions we can see the formation of shock waves and rarefaction waves. These solutions are only an approximation of real solutions. For example, the solutions after $t = 0$ in **Figure** 2.4 are not exact jumps, while the theoretical solution to the LWR model with initial conditions (2.3) is still a jump at any time. However as $\Delta x \to 0$ and $\Delta t \to 0$, the solutions given by Godunov's method converge to the exact solutions.

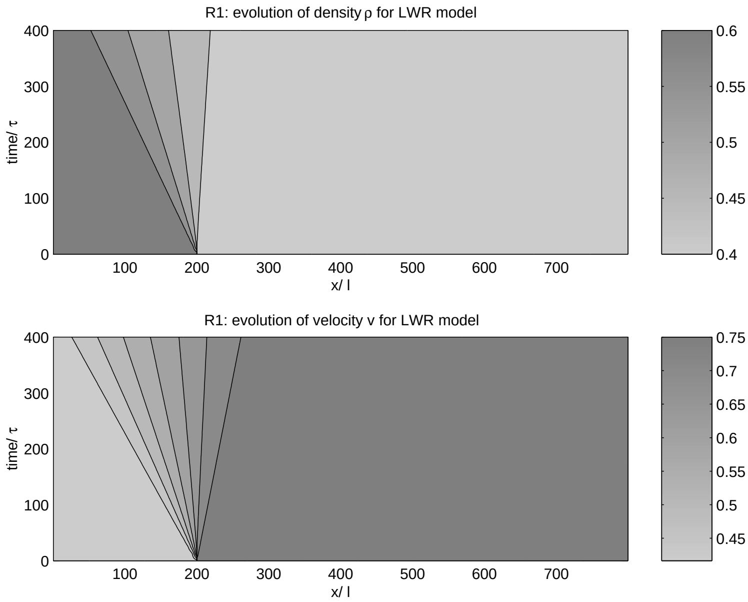

Figure 2.1: Rarefaction wave solution of the LWR model with initial data (2.3)

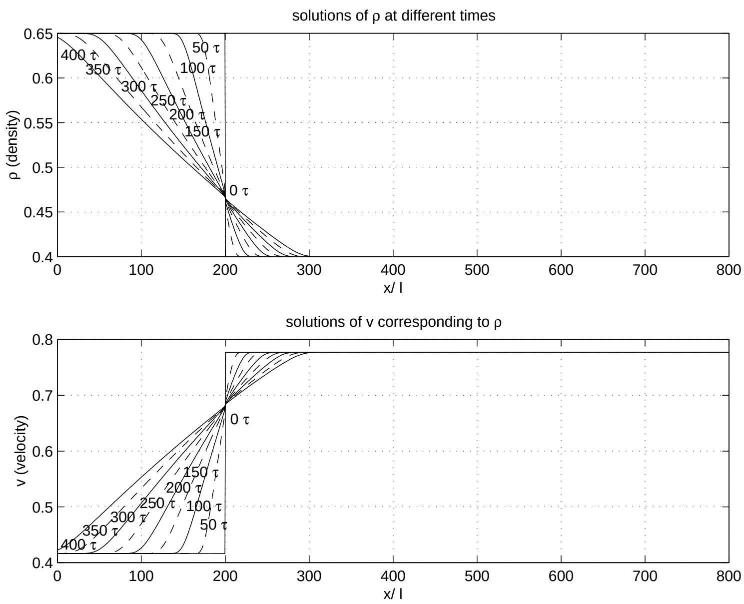

Figure 2.2: Solutions from **Figure** 2.1 at selected times

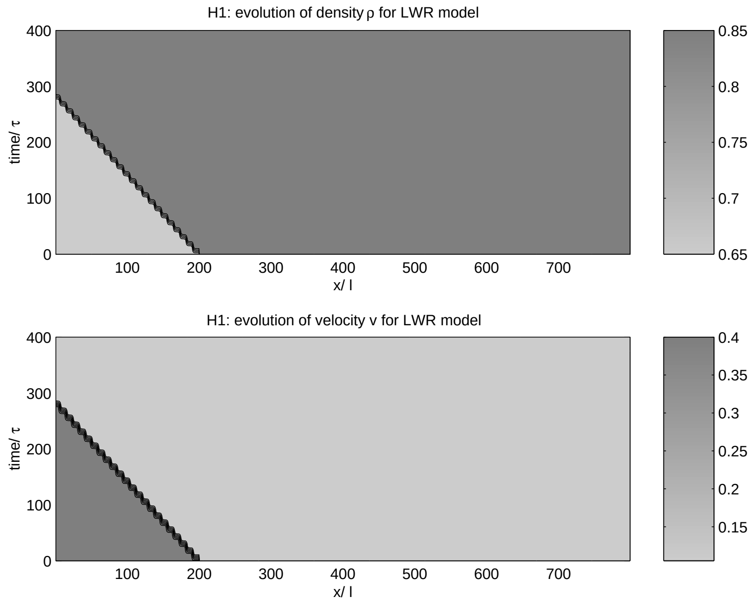

Figure 2.3: Shock wave solution of the LWR model with initial data (2.3)

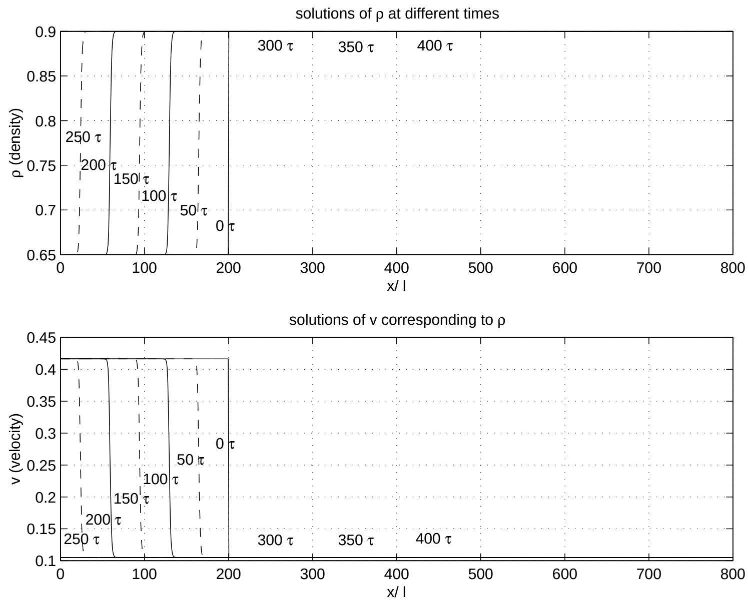

Figure 2.4: Solutions from **Figure** 2.3 at selected times

Chapter 3

Zhang's Second-Order Traffic Flow Model and Its Numerical Solutions

3.1 Introduction

A theory of non-equilibrium traffic flow has been developed by Zhang (1998), and in Zhang (2000a) he developed the Godunov-type finite difference equations (FDE) for this model. Zhang's model is a second-order model, and can be written in the conservation form

$$\begin{pmatrix} \rho \\ v \end{pmatrix}_t + \begin{pmatrix} \rho v \\ \frac{v^2}{2} + \phi(\rho) \end{pmatrix}_x = \begin{pmatrix} 0 \\ \frac{v_*(\rho) - v}{\tau} \end{pmatrix}, \tag{3.1}$$

where $\phi(\rho)$ is a velocity flux function and defined as

$$\phi'(\rho) = \frac{c^2(\rho)}{\rho} = \rho(v_*'(\rho))^2. \tag{3.2}$$

Here $c(\rho) = -\rho v_*'(\rho)$ is the traffic sound speed.

In (3.1), $v_*(\rho)$ is the equilibrium speed. Some often-used equilibrium travel speed functions are listed along with the corresponding velocity flux functions $\phi(\rho)$ as follows:

Functions	$v_*(\rho)$	$\phi(\rho)$
Greenshields	$v_f(1-\rho/\rho_j)$	$\frac{{v_f}^2}{2{\rho_j}^2}\rho^2$
Polynomial	$v_f(1-(\rho/\rho_j)^n), n>1$	$\frac{v_f^2}{2}(\rho/\rho_j)^{2n}$
Greenberg	$v_0\ln(\rho_j/\rho)$	$v_0^2\ln(\rho)$
Underwood	$v_f\exp(-\rho/\rho_j)$	$-v_f^2(1+\rho/\rho_j)\exp(-\rho/\rho_j)$
Newell	$v_f[1-\exp(\frac{\vert c_j\vert}{v_f}(1-\rho_j/\rho))]$	$\frac{v_f^2}{2}(\frac{\rho_j\vert c_j\vert}{v_f}\frac{1}{\rho}+\frac{1}{2})\exp(2\frac{\vert c_j\vert}{v_f}(1-\rho_j/\rho))$

The equilibrium travel speed v_* is decreasing with respect to traffic density; i.e., ${v_*}'(\rho)<0$. The fundamental diagram $f_*(\rho)\equiv\rho v_*(\rho)$ is concave; i.e., $f_*''(\rho)<0$. In (3.1), τ is the relaxation time and the relaxation term $\frac{v_*(\rho)-v}{\tau}$ constrains the difference between the real travel speed v and the equilibrium travel speed v_*. When the relaxation term is 0, Zhang's model reduces to the LWR model:

$$\rho_t+(\rho v_*)_x \;=\; 0. \tag{3.3}$$

Zhang's model has three different wave velocities (relative to the road): A first-order wave velocity and two second-order wave velocities. The first-order wave velocity is the wave velocity of the corresponding LWR model:

$$\lambda_*(\rho) \;=\; v_*(\rho)-c(\rho)=v_*(\rho)+\rho{v_*}'(\rho). \tag{3.4}$$

The two second-order wave velocities are

$$\lambda_{1,2}(\rho,v) \;=\; v\mp c(\rho)=v\pm\rho{v_*}'(\rho). \tag{3.5}$$

The relationship between these three wave speeds along (ρ,v_*) phase curves is that

$$\lambda_1=\lambda_*<\lambda_2. \tag{3.6}$$

The waves with wave speed λ_1 are called 1-waves; similarly the waves with wave speed λ_2 is called 2-waves. Since $\rho,v\ge 0$ and $v_*'<0$, the 2-wave speed $\lambda_2>0$ for any ρ,v.

Since Zhang's model is a hyperbolic system of conservation laws with a relaxation term, the system is stable when (Liu, 1979, 1987; Chen et al., 1994)

$$\lambda_1\le\lambda_*\le\lambda_2.$$

This condition is satisfied by Zhang's model. Thus Zhang's model is always stable.

In the following sections we study Godunov-type methods and use them to solve (3.1) numerically. In section 2 we discuss Godunov's method and properties of Zhang's model. In section 3 we present a second-order Godunov method. In Section 4 we solve the Riemann problems numerically and discuss the order of accuracy for different methods.

3.2 Godunov's method

A Godunov-type finite difference method for Zhang's model was first presented in (Zhang, 2000a). In this section we review this Godunov method and solve the associated Riemann problem.

The Godunov-type FDEs for Zhang's model are

$$\frac{\rho_i^{j+1}-\rho_i^j}{k}+\frac{\rho_{i+1/2}^{*j}v_{i+1/2}^{*j}-\rho_{i-1/2}^{*j}v_{i-1/2}^{*j}}{h} = 0, \tag{3.7}$$

$$\frac{v_i^{j+1}-v_i^j}{k}+\frac{\frac{(v_{i+1/2}^{*j})^2}{2}+\phi(\rho_{i+1/2}^{*j})-\frac{(v_{i-1/2}^{*j})^2}{2}-\phi(\rho_{i-1/2}^{*j})}{h} = \frac{v_*(\rho_i^{j+1})-v_i^{j+1}}{\tau}. \tag{3.8}$$

In these FDEs, ρ_i^j is the average of ρ in cell i at time step j; i.e.,

$$\rho_i^j = \frac{1}{h}\int_{x_{i-1/2}}^{x_{i+1/2}} \rho(x,t_j)dx. \tag{3.9}$$

Similarly v_i^j is the average of v. We use $\rho_{i+1/2}^{*j}$ as the average of ρ through the cell boundary $x_{i+1/2}$ over the time interval (t_j,t_{j+1}), i.e.,

$$\rho_{i+1/2}^{*j} = \frac{1}{k}\int_{t_j}^{t_{j+1}} \rho(x_{i+1/2},t)dt. \tag{3.10}$$

Similarly we define $v_{i+1/2}^{*j}, \rho_{i-1/2}^{*j}, v_{i-1/2}^{*j}$ as boundary averages.

By measuring the source term with values at time t_{j+1}, we write the evolution equations for Zhang's model as

$$\rho_i^{j+1} = \rho_i^j - \frac{k}{h}(\rho_{i+1/2}^{*j} v_{i+1/2}^{*j} - \rho_{i-1/2}^{*j} v_{i-1/2}^{*j}) \tag{3.11}$$

$$\begin{aligned} v_i^{j+1} &= \frac{1}{(1+\frac{k}{\tau})}\{v_i^j - \frac{k}{h}[\frac{(v_{i+1/2}^{*j})^2}{2} + \phi(\rho_{i+1/2}^{*j}) - \frac{(v_{i-1/2}^{*j})^2}{2} - \phi(\rho_{i-1/2}^{*j})] \\ &\quad + \frac{k}{\tau} v_*(\rho_i^{j+1})\} \end{aligned} \tag{3.12}$$

Provided traffic conditions (ρ, v) at time t_j, traffic conditions at time t_{j+1} can be calculated if we know the boundary averages $\rho_{i+1/2}^{*j}, v_{i+1/2}^{*j}, \rho_{i-1/2}^{*j}, v_{i-1/2}^{*j}$. The computation of $\rho_{i+1/2}^{*j}, v_{i+1/2}^{*j}$ at the cell boundary $x_{i+1/2}$ during the time interval (t_j, t_{j+1}) depends on a Riemann problem for (3.1) with the following initial conditions

$$u_{i+1/2}(x, t_j) = \begin{cases} U_l, & \text{if } x - x_{i+1/2} < 0 \\ U_r, & \text{if } x - x_{i+1/2} > 0 \end{cases}, \tag{3.13}$$

where we define the state variable $u(x,t) = (\rho, v)$, $U_i^j = (\rho_i^j, v_i^j) = u(x_i, t_j)$ and left and right states $U_l = (\rho_l, v_l), U_r = (\rho_r, v_r)$. In a first-order Godunov method, we use the cell averages $\rho_l = \rho_i^j, v_l = v_i^j$ as the left side (upstream) traffic conditions and $\rho_r = \rho_{i+1}^j, v_r = v_{i+1}^j$ as the right side (downstream) conditions. In a second-order Godunov method, we use higher-order approximations to the left and right states. (For details for a second-order Godunov method, refer to Section 3.3.)

Here we have neglected the relaxation term in (3.1) when solving the Riemann problem. This Riemann problem has been discussed by Zhang (1999a), and the solutions to the boundary averages are provided there. The solutions are self-similar and can be expressed in the form of

$$\psi(\frac{x - x_{i+1/2}}{t}; U_r, U_l).$$

3.2.1 Solutions of the boundary averages

There are 8 types of wave solutions to the Riemann problem, which are combinations of two 1-waves and two 2-waves. The calculation of the boundary averages depend on the type of solutions. The formula for calculating the boundary averages are listed as follows.

1. The wave solution is a 1-shock when the initial conditions satisfy

$$\text{H1: } v_r - v_l = -\sqrt{\frac{2(\rho_l - \rho_r)(\phi(\rho_l) - \phi(\rho_r))}{\rho_l + \rho_r}}, \quad \rho_r > \rho_l,\ v_r < v_l. \tag{3.14}$$

The wave speed is

$$s = \frac{\rho_r v_r - \rho_l v_l}{\rho_r - \rho_l} \tag{3.15}$$

The boundary averages $(\rho^{*j}_{i+1/2}, v^{*j}_{i+1/2})$ are given in the following table:

	$s = \frac{\rho_r v_r - \rho_l v_l}{\rho_r - \rho_l}$	$\rho^{*j}_{i+1/2}$	$v^{*j}_{i+1/2}$
H1	$s > 0$	ρ_l	v_l
	$s < 0$	ρ_r	v_r
	$s = 0$	$\frac{\rho_l+\rho_r}{2}$	$\frac{v_l+v_r}{2}$

2. The wave solution is a 2-shock when the initial states satisfy

$$\text{H2: } v_r - v_l = -\sqrt{\frac{2(\rho_l - \rho_r)(\phi(\rho_l) - \phi(\rho_r))}{\rho_l + \rho_r}}, \quad \rho_r < \rho_l,\ v_r < v_l \tag{3.16}$$

The wave speed is

$$s = \frac{\rho_r v_r - \rho_l v_l}{\rho_r - \rho_l} > 0. \tag{3.17}$$

The boundary averages $(\rho^{*j}_{i+1/2}, v^{*j}_{i+1/2})$ are given in the following table:

	$s = \frac{\rho_r v_r - \rho_l v_l}{\rho_r - \rho_l}$	$\rho^{*j}_{i+1/2}$	$v^{*j}_{i+1/2}$
H2	$s > 0$	ρ_l	v_l

3. The wave solution is a 1-rarefaction when the initial states satisfy

$$\text{R1: } v_r - v_l = v_*(\rho_r) - v_*(\rho_l), \quad \rho_r < \rho_l,\ v_r > v_l \tag{3.18}$$

The characteristic speed of a 1-rarefaction wave is

$$\lambda_1(\rho, v) = v + \rho {v_*}'(\rho) \tag{3.19}$$

The boundary averages are the left state when $\lambda_1(\rho_l, v_l) > 0$, similarly they are the right state when $\lambda_1(\rho_r, v_r) < 0$. Otherwise, $(\rho^{*j}_{i+1/2}, v^{*j}_{i+1/2})$ are the solutions of the equations

$$\lambda_1(\rho^{*j}_{i+1/2}, v^{*j}_{i+1/2}) = \rho^{*j}_{i+1/2} {v_*}'(\rho^{*j}_{i+1/2}) + v^{*j}_{i+1/2} = 0 \tag{3.20}$$

$$v^{*j}_{i+1/2} - v_l = v_*(\rho^{*j}_{i+1/2}) - v_*(\rho_l). \tag{3.21}$$

We simplify equations (3.20,3.21) as

$$\lambda_*(\rho^{*j}_{i+1/2}) = v_*(\rho_l) - v_l \equiv \Delta v \tag{3.22}$$

$$v^{*j}_{i+1/2} = v_*(\rho^{*j}_{i+1/2}) - \Delta v. \tag{3.23}$$

The boundary averages $(\rho^{*j}_{i+1/2}, v^{*j}_{i+1/2})$ are given in the following table:

	λ_1	$\rho^{*j}_{i+1/2}$	$v^{*j}_{i+1/2}$
R1	$\lambda_1(\rho_l, v_l) > 0$	ρ_l	v_l
	$\lambda_1(\rho_r, v_r) < 0$	ρ_r	v_r
	o.w.	solution to (3.22,3.23)	

4. The wave solution is a 2-rarefaction when the initial states satisfy

$$\text{R2: } v_r - v_l = v_*(\rho_l) - v_*(\rho_r), \quad \rho_r > \rho_l,\ v_r > v_l \tag{3.24}$$

The characteristic speed of the 2-rarefaction wave is

$$\lambda_2(\rho, v) = v - \rho {v_*}'(\rho) > 0. \tag{3.25}$$

The solutions of $(\rho^{*j}_{i+1/2}, v^{*j}_{i+1/2})$ are given in the following table:

	λ_2	$\rho^{*j}_{i+1/2}$	$v^{*j}_{i+1/2}$
R2	$\lambda_2 > 0$	ρ_l	v_l

5. The wave solution is a 1-rarefaction + 2-rarefaction when there exists an intermediate state (ρ_m, v_m) satisfying

$$\text{R1: } v_m - v_l = v_*(\rho_m) - v_*(\rho_l), \quad \rho_m < \rho_l,\ v_m > v_l \tag{3.26}$$

$$\text{R2: } v_r - v_m = v_*(\rho_m) - v_*(\rho_r), \quad \rho_r > \rho_m,\ v_r > v_m. \tag{3.27}$$

That is to say, ρ_m satisfies

$$2 * v_*(\rho_m) - v_*(\rho_l) - v_*(\rho_r) - (v_r - v_l) = 0 \tag{3.28}$$

in which $\rho_m < \rho_l, \rho_m < \rho_r$. We can write v_m as

$$v_m = v_*(\rho_m) + v_l - v_*(\rho_l). \tag{3.29}$$

The boundary averages $(\rho^{*j}_{i+1/2}, v^{*j}_{i+1/2})$ are given in the following table:

	λ_1	$\rho^{*j}_{i+1/2}$	$v^{*j}_{i+1/2}$
R1-R2	$\lambda_1(\rho_l, v_l) > 0$	ρ_l	v_l
	$\lambda_1(\rho_m, v_m) < 0$	ρ_m	v_m
	o.w.	solution to (3.22,3.23)	

6. The wave solution is a 1-rarefaction + 2-shock when there exists an intermediate state (ρ_m, v_m) satisfying

$$\text{R1: } v_m - v_l = v_*(\rho_m) - v_*(\rho_l) \quad , \rho_m < \rho_l,\ v_m > v_l \tag{3.30}$$

$$\text{H2: } v_r - v_m = -\sqrt{\frac{2(\rho_m - \rho_r)(\phi(\rho_m) - \phi(\rho_r))}{\rho_m + \rho_r}} \quad , \rho_r < \rho_m,\ v_r < v_m. \tag{3.31}$$

That is to say, ρ_m satisfies

$$v_*(\rho_m) - v_*(\rho_l) - \sqrt{\tfrac{2(\rho_m-\rho_r)(\phi(\rho_m)-\phi(\rho_r))}{\rho_m+\rho_r}} - (v_r - v_l) \quad = 0 \tag{3.32}$$

in which $\rho_r < \rho_m < \rho_l$. We can write v_m as

$$v_m = v_*(\rho_m) + v_l - v_*(\rho_l). \tag{3.33}$$

The boundary averages $(\rho^{*j}_{i+1/2}, v^{*j}_{i+1/2})$ are given as the following

	λ_1	$\rho^{*j}_{i+1/2}$	$v^{*j}_{i+1/2}$
R1-H2	$\lambda_1(\rho_l, v_l) > 0$	ρ_l	v_l
	$\lambda_1(\rho_m, v_m) < 0$	ρ_m	v_m
	o.w.	solution to (3.22,3.23)	

7. The wave solution is a 1-shock + 2-shock when there exists an intermediate state (ρ_m, v_m) satisfying

$$\text{H1: } v_m - v_l = \quad -\sqrt{\tfrac{2(\rho_l-\rho_m)(\phi(\rho_l)-\phi(\rho_m))}{\rho_l+\rho_m}} \quad , \rho_m > \rho_l,\ v_m < v_l \tag{3.34}$$

$$\text{H2: } v_r - v_m = \quad -\sqrt{\tfrac{2(\rho_m-\rho_r)(\phi(\rho_m)-\phi(\rho_r))}{\rho_m+\rho_r}} \quad , \rho_r < \rho_m,\ v_r < v_m. \tag{3.35}$$

That is to say, ρ_m satisfies

$$-\sqrt{\tfrac{2(\rho_l-\rho_m)(\phi(\rho_l)-\phi(\rho_m))}{\rho_l+\rho_m}} - \sqrt{\tfrac{2(\rho_m-\rho_r)(\phi(\rho_m)-\phi(\rho_r))}{\rho_m+\rho_r}} - (v_r - v_l) \quad = 0 \tag{3.36}$$

in which $\rho_m > \rho_l, \rho_m > \rho_r$. We can compute v_m as

$$v_m = -\sqrt{\frac{2(\rho_l-\rho_m)(\phi(\rho_l)-\phi(\rho_m))}{\rho_l+\rho_m}} + v_l. \tag{3.37}$$

The boundary averages $(\rho^{*j}_{i+1/2}, v^{*j}_{i+1/2})$ are given in the following table:

	$s = \frac{\rho_m v_m - \rho_l v_l}{\rho_r - \rho_l}$	$\rho^{*j}_{i+1/2}$	$v^{*j}_{i+1/2}$
H1-H2	$s > 0$	ρ_l	v_l
	$s < 0$	ρ_m	v_m
	$s = 0$	$\frac{\rho_l+\rho_m}{2}$	$\frac{v_l+v_m}{2}$

8. The wave solution is a 1-shock + 2-rarefaction when there exists an intermediate state (ρ_m, v_m) satisfying

$$\begin{aligned}
&\text{H1: } v_m - v_l = && -\sqrt{\tfrac{2(\rho_l-\rho_m)(\phi(\rho_l)-\phi(\rho_m))}{\rho_l+\rho_m}} && , \rho_m > \rho_l,\ v_m < v_l && (3.38)\\
&\text{R2: } v_r - v_m = && v_*(\rho_m) - v_*(\rho_r) && , \rho_r > \rho_m,\ v_r > v_m. && (3.39)
\end{aligned}$$

That is to say, ρ_m satisfies

$$-\sqrt{\tfrac{2(\rho_l-\rho_m)(\phi(\rho_l)-\phi(\rho_m))}{\rho_l+\rho_m}} + v_*(\rho_m) - v_*(\rho_r) - (v_r - v_l) \;= 0 \quad (3.40)$$

in which $\rho_m > \rho_l, \rho_m > \rho_r$. We compute v_m as

$$v_m = -\sqrt{\frac{2(\rho_l-\rho_m)(\phi(\rho_l)-\phi(\rho_m))}{\rho_l+\rho_m}} + v_l. \quad (3.41)$$

The boundary averages $(\rho^{*j}_{i+1/2}, v^{*j}_{i+1/2})$ are given in the following table:

	$s = \frac{\rho_m v_m - \rho_l v_l}{\rho_r - \rho_l}$	$\rho^{*j}_{i+1/2}$	$v^{*j}_{i+1/2}$
H1-R2	$s > 0$	ρ_l	v_l
	$s < 0$	ρ_m	v_m
	$s = 0$	$\frac{\rho_l+\rho_m}{2}$	$\frac{v_l+v_m}{2}$

3.2.2 Some points concerning the implementation of the Godunov method

In subsection 3.2.1 above, we studied the solutions of the boundary averages. We now discuss how to get a stable, convergent and efficient numerical method.

In a linear hyperbolic system, Godunov's method is stable and convergent if the Courant-Friedrichs-Lewy (CFL) number is less than unity. Similarly we require the CFL number be less than unity for Zhang's model; i.e.,

$$\max\left|\frac{k}{h}\lambda_2(\rho, v)\right| \;\leq\; 1 \quad (3.42)$$

where $\lambda_2(\rho, v) = v - \rho {v_*}'(\rho)$ has the bigger magnitude of two wave velocities.

There are two types of boundary conditions (BC) : Dirichlet BC and Neumann (or natural) BC. If the interval for x is $[a, b]$, we will impose boundary condition on $u(a - \frac{h}{2}, t_j)$ and $u(b + \frac{h}{2})$ instead of the real boundary $x = a$ and $x = b$. This is to say we have to solve a Riemann problem to get the fluxes on both the end boundaries instead of imposing boundary conditions directly on those fluxes. [1]

The source term, $s(u) = (0, \frac{v_*(\rho) - v}{\tau})$, doesn't involve spatial gradients and therefore remains bounded as terms on the left hand-side of (3.1) go to ∞. We approximate the source term implicitly with $s(U_i^{j+1})$ or $s(\frac{U_i^{j+1} + U_i^j}{2})$ in order to improve the stability property of the Godunov method. However, when the source term is stiff; i.e., when τ is small, the problem of numerical instability may arise. In this case we use a much smaller time increment $k \ll \tau$.

The solution to the Riemann problem is important both theoretically and computationally. One can compute the numerical solutions when all of the Riemann problems are well-posed and solvable at each step of the iteration. However, when the left and right states for a Riemann problem are far from each other, the intermediate state (ρ_m, v_m) for the wave solutions may be out of domain of validity, e.g., $\rho_m < 0$. In this case, we have a "vacuum problem" and hence the numerical solutions can not be uniquely determined.

The cost of solving the Riemann problem determines the computational efficiency of the numerical method. Here we propose improvements to the computational efficiency for Zhang's model. In Godunov's methods for Zhang's model, most of the calculations are basic arithmetic computations except the calculation of the intermediate state (ρ_m, v_m) in equations (3.28),(3.32),(3.36) and (3.40) and the solutions of equations (3.22) and (3.23)). Given (ρ_l, v_l) and (ρ_r, v_r), the nonlinear algebraic equations (3.28),(3.32),(3.36) and (3.40) can all be written in the form of $g(\rho_m) = 0$. The functions $g(\rho_m)$ for these equations are all monotonically decreasing in the interval of

[1] For the detailed discussions on treatment of boundary conditions, refer to (Zhang, 2000a).

validity of ρ_m. To find $\rho^{*j}_{i+1/2}$ from equation (3.22), we define a function

$$g(\rho) \quad = \quad \lambda_*(\rho) - \Delta v, \quad \rho_r \ (\rho_m \text{ for R1-R2,R1-H2}) < \rho < \rho_l. \tag{3.43}$$

Since $f_*(\rho)$ is concave and $\lambda_*(\rho) = f'_*(\rho)$, we find $\lambda_*(\rho)$ and $g(\rho)$ are decreasing. Here we chose secant method to solve these equations since it is very efficient when the associated functions are monotonically decreasing.

3.3 A Second-order Godunov Method

In this section we introduce a second-order finite difference method for Zhang's model. This method is a two-stage predictor/corrector method. In this method, (3.1) is decoupled into two nonlinear scalar equations in each interval $(x_{i-1/2}, x_{i+1/2})$ at time t_j and the predictor/corrector procedures are applied to those scalar functions.

We can write Zhang's model as:

$$u_t + A(u)u_x \quad = \quad s(u) \tag{3.44}$$

where

$$u \quad = \quad \begin{pmatrix} \rho(x,t) \\ v(x,t) \end{pmatrix} \tag{3.45}$$

and

$$A(u) \quad = \quad \begin{pmatrix} v & \rho \\ \rho {v_*'}^2 & v \end{pmatrix} \tag{3.46}$$

The two eigenvalues and corresponding eigenvectors are

$$\begin{aligned} \lambda_1(u) &= v + \rho v_*(\rho), \quad r_1(u) = [1, {v_*}'(\rho)]^t, \\ \lambda_2(u) &= v - \rho {v_*}'(\rho), \quad r_2(u) = [1, -{v_*}'(\rho)]^t. \end{aligned} \tag{3.47}$$

We diagonalize $A(u)$ by

$$T^{-1}(u)A(u)T(u) \quad = \quad \begin{pmatrix} \lambda_1(u) & 0 \\ 0 & \lambda_2(u) \end{pmatrix} \equiv \Lambda(u), \tag{3.48}$$

where the transformation matrix $T(u)$ is

$$T(u) = \begin{pmatrix} 1 & 1 \\ {v_*}'(\rho) & -{v_*}'(\rho) \end{pmatrix}. \tag{3.49}$$

Letting $W = T^{-1}(u)u$, Zhang's model (3.1) under the transformation becomes

$$W_t + \Lambda(u)W_x = T^{-1}(u)s(u). \tag{3.50}$$

For the solution $w(x,t)$ to a scalar equation $w_t + \lambda(w)w_x = 0$, the first-order Godunov method uses a step function $w_I(x,t_j)$ to interpolate the solution, i.e.,

$$w_I(x,t_j) = w_i^j, \text{ if } x_{i-1/2} < x \leq x_{i+1/2}. \tag{3.51}$$

In a first-order Godunov method, the Riemann problem has the following jump initial conditions:

$$\begin{aligned} w_{i+1/2}^{j,L} &= w_i^j \\ w_{i-1/2}^{j,R} &= w_i^j. \end{aligned} \tag{3.52}$$

For a second-order Godunov method, we interpolate the initial condition with a piecewise linear function

$$w_I(x,t_j) = w_i^j + \frac{(x-ih)}{h}\Delta^{VL}w_i^j, \text{ if } x_{i-1/2} < x \leq x_{i+1/2}. \tag{3.53}$$

Then we do a half-step prediction

$$\begin{aligned} w_{i+1/2}^{j+1/2,L} &= w_i^j + \tfrac{1}{2}(1 - \lambda(w_i^j)\tfrac{k}{h})\Delta^{VL}w_i^j \\ w_{i-1/2}^{j+1/2,R} &= w_i^j - \tfrac{1}{2}(1 + \lambda(w_i^j)\tfrac{k}{h})\Delta^{VL}w_i^j, \end{aligned} \tag{3.54}$$

where $\Delta^{VL}w_i^j$ is the van Leer slope defined as (all subscripts j have been suppressed)

$$\Delta^{VL}w_i = \begin{cases} S_i \cdot \min(2|w_{i+1}-w_i|, 2|w_i - w_{i-1}|, \tfrac{1}{2}|w_{i+1}-w_{i-1}|), & \xi > 0 \\ 0, & \text{otherwise} \end{cases}$$

$$S_i = \operatorname{sign}(w_{i+1} - w_{i-1}) \tag{3.55}$$

$$\xi = (w_{i+1} - w_i)\cdot(w_i - w_{i-1}) \tag{3.56}$$

The van Leer slope limiter ensures that the method remains second order when the solution $w(x,t)$ is smooth and eliminates Gibb's phenomenon at discontinuities.

We apply the procedure above to the two scalar equations of the related homogeneous 2×2 system in (3.50) to obtain $W_{i+1/2}^{j+1/2,L}$ and $W_{i-1/2}^{j+1/2,R}$. Given the half-step values of $W_{i+1/2}^{j+1/2,L}$ and $W_{i-1/2}^{j+1/2,R}$, $U_{i+1/2}^{j+1/2,L}$ and $U_{i-1/2}^{j+1/2,R}$ can be calculated by an inverse transformation:

$$\begin{aligned} U_{i+1/2}^{j+1/2,L} &= T(U_i^j)W_{i+1/2}^{j+1/2,L} \\ U_{i-1/2}^{j+1/2,R} &= T(U_i^j)W_{i-1/2}^{j+1/2,R} \end{aligned} \tag{3.57}$$

We then solve the Riemann problem to find the boundary averages.

3.4 Numerical Solutions of Zhang's model

Based on the discussions in the former sections, we carry out some numerical computations to test the validity of the Godunov method and the properties of Zhang's model.

Here we use Newell's equilibrium model,

$$v_*(\rho) = v_f\left(1 - \exp\{\frac{|c_j|}{v_f}(1-\rho_j/\rho)\}\right). \tag{3.58}$$

and set $v_f = 1, c_j = 1, \rho_j = 1$ to get the standardized equilibrium relationship:

$$v_*(\rho) = 1 - \exp(1 - \frac{1}{\rho}) \tag{3.59}$$

The domain for ρ is $0 \leq \rho \leq 1$[2], the range for v_* is the same. The traffic flow rate is $f_* = \rho v_*$. The equilibrium travel speed $v_*(\rho)$ and flow rate $f_*(\rho)$ are shown in **Figure** 3.1.

The subcharacteristic; i.e., the first-order characteristic velocity, (i.e., the wave velocity of the corresponding LWR model) is

$$\lambda_* = 1 - (1 + \frac{1}{\rho})\exp(1 - \frac{1}{\rho}),$$

[2] We use the limit of v_* when $\rho \to 0$ as its value at $\rho = 0$.

and the eigenvalues are

$$\lambda_{1,2} = v \pm \frac{1}{\rho} \exp{(1 - \frac{1}{\rho})}.$$

When $0 \leq \rho \leq 1$, we have

$$|\lambda_2| < |v| + 1.$$

The CFL condition number is defined as:

$$\max |\frac{k}{h}\lambda_2(\rho, v)| \leq \frac{k}{h}(\max v + 1). \tag{3.60}$$

Since the CFL number is no larger than 1, we find

$$k \leq \frac{h}{\max v + 1}. \tag{3.61}$$

In all of the computations that follow, we let $x \in [0l, 800l]$, where l is the unit of length. Here the number of grid points is denoted by N, and $h = \frac{800l}{N}$ is the space step. We let $T_0 = K\tau$ denote the final time (τ is the unit of time), and m the number of time steps and $k = \frac{K\tau}{m}$. From the CFL condition, we have

$$\frac{(\max v + 1)K}{800} \frac{N}{m} \frac{\tau}{l} \leq 1. \tag{3.62}$$

Setting $\tau = l = 10.0$, and $m = N$, CFL condition is not violated when $K \leq 400$ since $\max v < 1$.

3.4.1 Riemann solutions

In the following four computations we use the first-order Godunov method to examine different types of waves solutions. With four well-chosen jump initial conditions, we can observe four different type of waves H1-H2, R1-R2, R1-H2 and H1-R2. To prevent the 2-waves from relaxing to 1-waves in a short time, here we rescale the relaxation time $\tau \to 1000\tau$. For each computation we present a contour plot of both ρ and v until $T_0 = 400\tau$, and several 2-D curves at different time t have been selected from the contour plot.

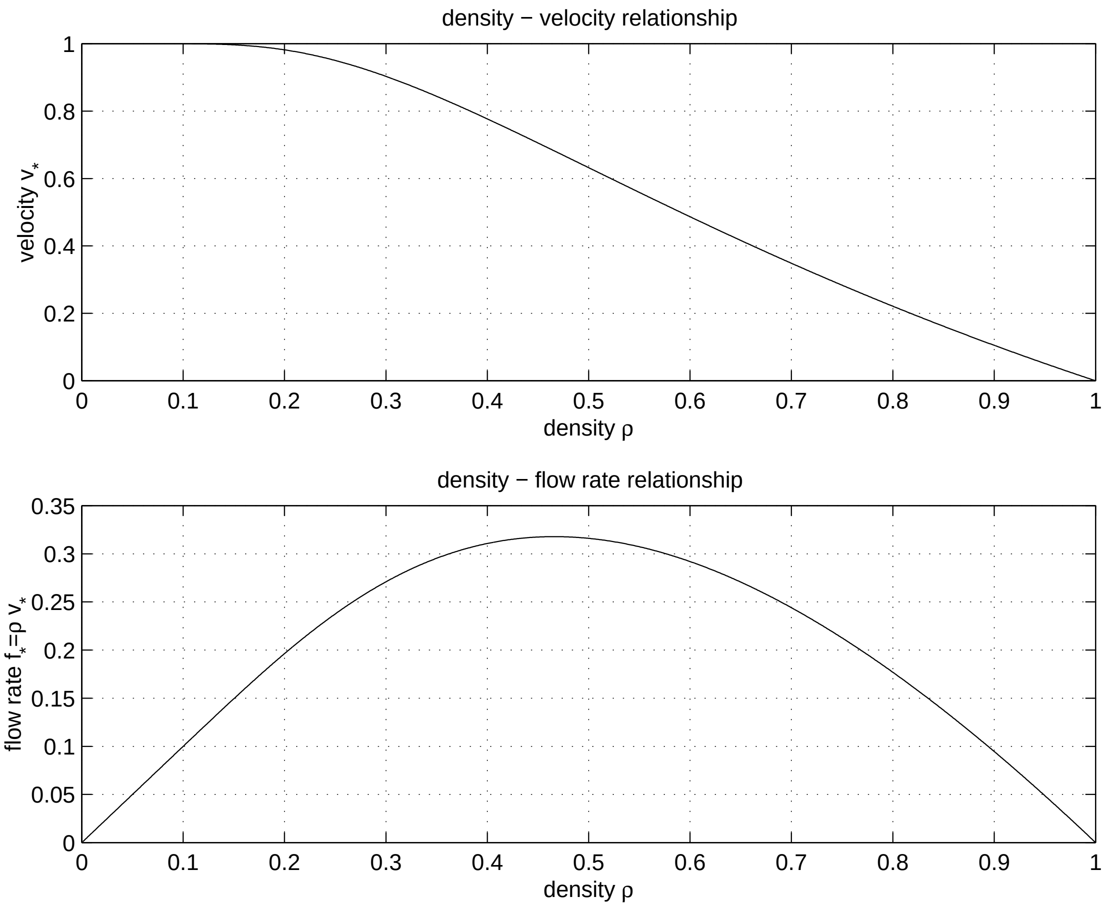

Figure 3.1: Newell's Equilibrium ρ–v_*/ ρ–f_* Relationship

Computation 1 We use the following initial conditions:

$$\rho(x,0) = 0.65, \qquad \forall x \in [0l, 800l] \tag{3.63}$$

$$v(x,0) = \begin{cases} v_*(0.65) & x \in [0l, 200l] \\ v_*(0.65) - 0.2 & \text{otherwise} \end{cases} \tag{3.64}$$

The solutions are of H1-H2 type, shown in **Figures** 3.2 and 3.3. These figures show that the downstream travel speed keeps increasing along with the propagation of the 2-shock wave. This is due to the effect of the relaxation term. We can predict that when the downstream travel speed reaches $v_*(0.65)$, which is the equilibrium travel speed with respect to the downstream traffic density $\rho = 0.65$, the 2-shock disappears and a 1-rarefaction wave forms.

Computation 2 We use the following initial conditions:

$$\rho(x,0) = 0.65, \qquad \forall x \in [0l, 800l] \tag{3.65}$$

$$v(x,0) = \begin{cases} v_*(0.65) & x \in [0l, 200l] \\ v_*(0.65) + 0.2 & \text{otherwise} \end{cases} \tag{3.66}$$

The solutions are of R1-R2 type, shown in **Figures** 3.4 and 3.5. These figures show that the downstream travel speed keeps decreasing along with the propagation of the 2-rarefaction wave. This is also due to the effect of the relaxation term, which will relax the 2-rarefaction wave to a 1-shock wave.

Computation 3 We use the following initial conditions:

$$\rho(x,0) = \begin{cases} 0.65 & x \in [0l, 200l] \\ 0.4 & \text{otherwise} \end{cases} \tag{3.67}$$

$$v(x,0) = v_*(0.65), \qquad \forall x \in [0l, 800l] \tag{3.68}$$

The solutions are of R1-H2 type, shown in **Figures** 3.6 and 3.7. Here the effect of the relaxation term will relax the 2-shock wave to a 1-rarefaction wave.

Computation 4 We use the following initial conditions:

$$\rho(x,0) = \begin{cases} 0.65 & x \in [0l, 200l] \\ 0.9 & \text{otherwise} \end{cases} \tag{3.69}$$

$$v(x,0) = v_*(0.65), \qquad \forall x \in [0l, 800l] \tag{3.70}$$

The the solutions are of H1-R2 type, shown in **Figures** 3.8 and 3.9. Here the effect of the relaxation term will relax the 2-rarefaction wave to a 1-shock wave.

3.4.2 A General Solution and Convergence Rates

In this subsection the relaxation time is no longer rescaled since we wish to observe the solutions to (3.1) for a longer time. Here we are interested in the solution for $0 \leq t \leq T_0 = 400\tau$.

Using the general initial condition

$$\rho(x,0) = 0.65 + \sin\left(\frac{2\pi x}{800l}\right)/4, \tag{3.71}$$

$$v(x,0) = v_*(\rho(x,0)) + 0.1, \qquad \forall x \in [0l, 800l], \tag{3.72}$$

we use the first-order Godunov method to obtain the solutions shown in **Figures** 3.10 and 3.11. From these figures we see a shock wave forms at the downstream section, and a complicated combination of rarefaction waves forms in the upstream section. The solutions also show that ρ-v are in equilibrium by $t = 100\tau$, i.e., $v = v_*(\rho)$, due to the effect of the relaxation term, although the initial condition is not in equilibrium.

Next, we compute the convergence rate for the first- and second-order methods with Neumann boundary conditions with initial conditions (3.71,3.72). The convergence rate is calculated from the comparison between the solution on different grids. The grid numbers $2N$ and N generate different grid sizes: $\frac{h}{2}$ and h. We denote the solutions at time T_0 as $(U_i^{2N})_{i=1}^{2N}$ and $(U_i^N)_{i=1}^{N}$ respectively, and define the difference

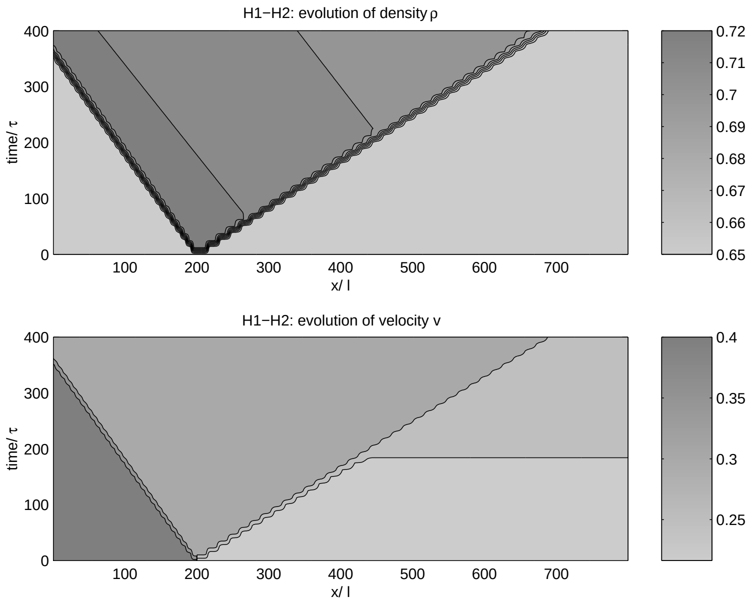

Figure 3.2: Left-Shock-Right-Shock Wave Solution

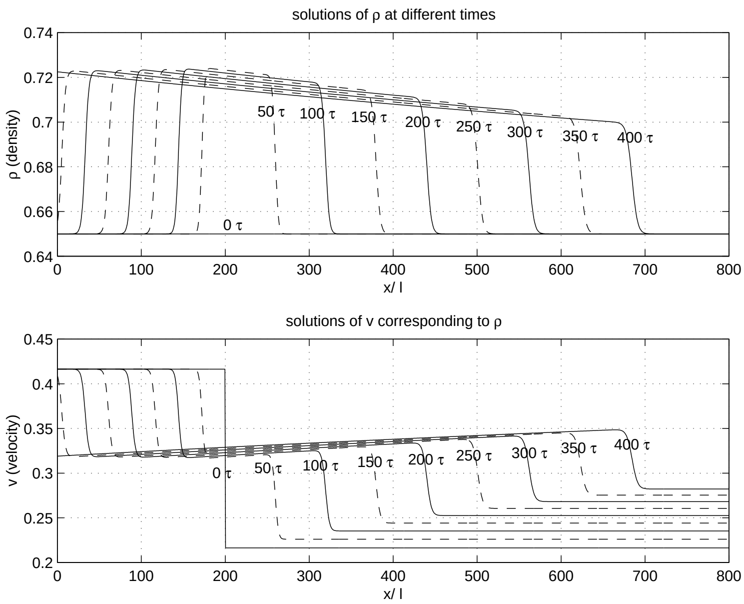

Figure 3.3: H1-H2 Solutions from at Selected Times

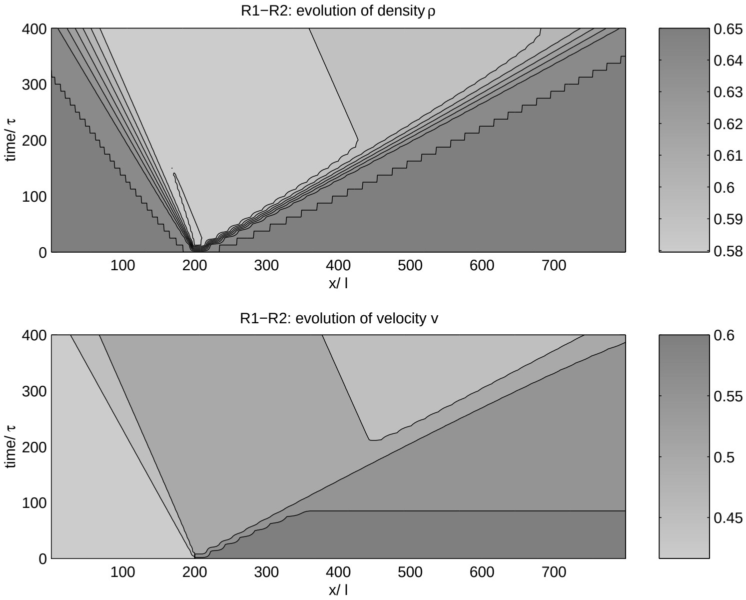

Figure 3.4: Left-Rarefaction-Right-Rarefaction Wave Solution

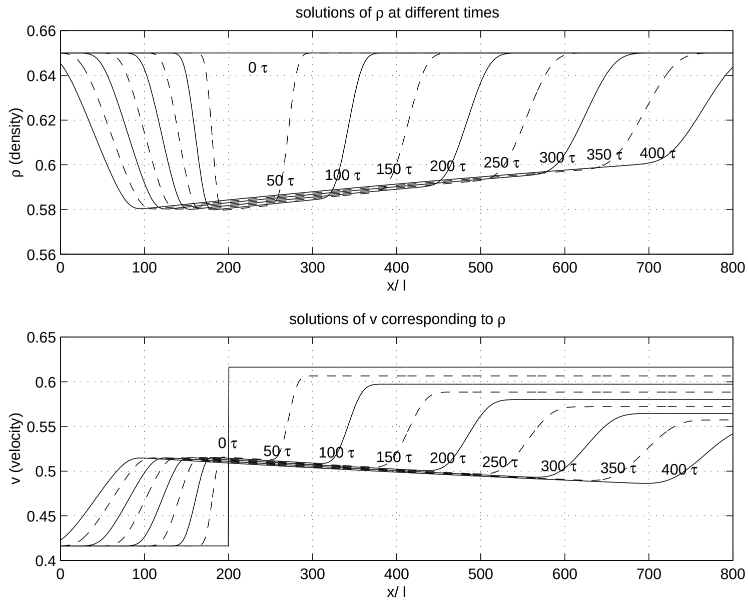

Figure 3.5: R1-R2 Solutions at Selected Times

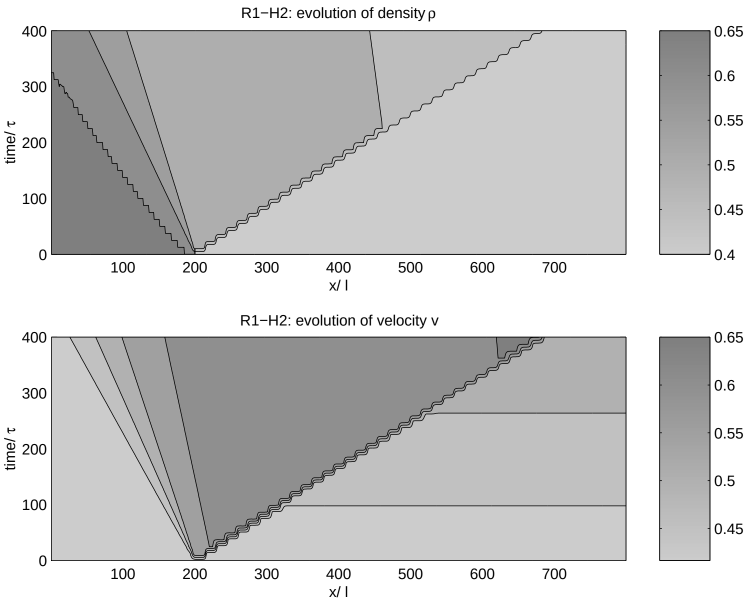

Figure 3.6: Left-Rarefaction-Right-Shock Wave Solution

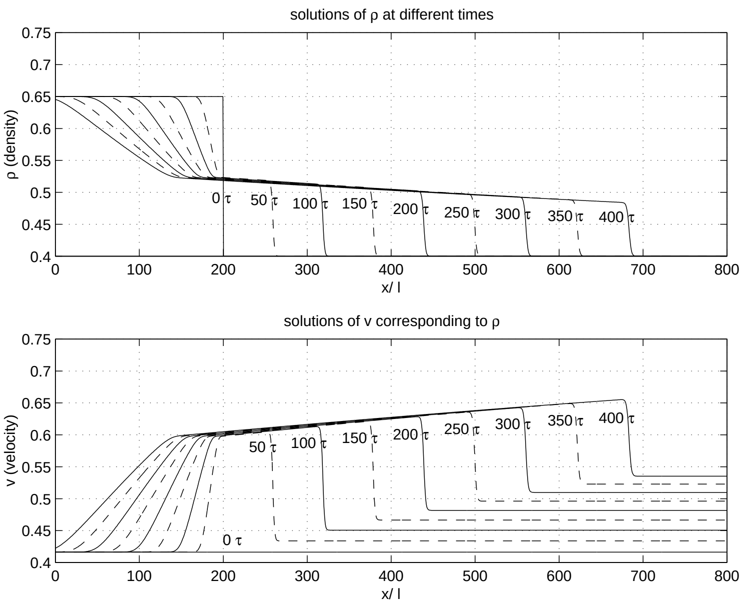

Figure 3.7: R1-H2 Solutions at Selected Times

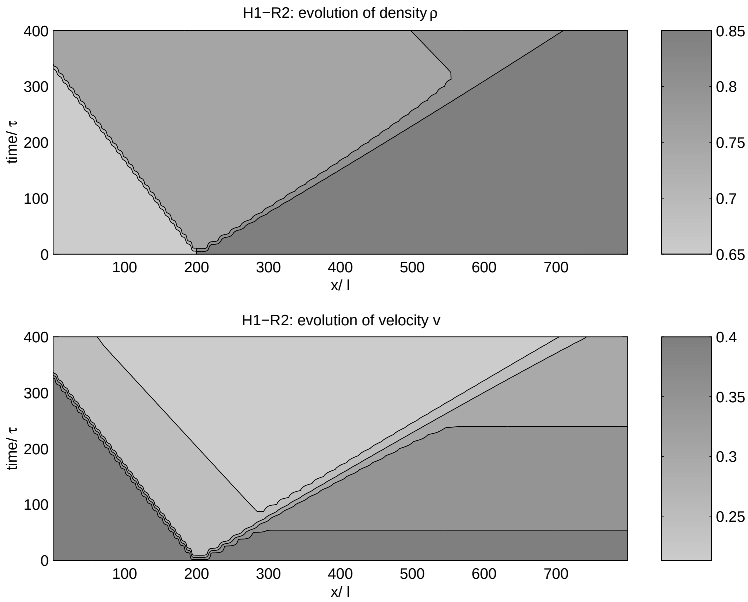

Figure 3.8: Left-Shock-Right-Rarefaction Wave Solution

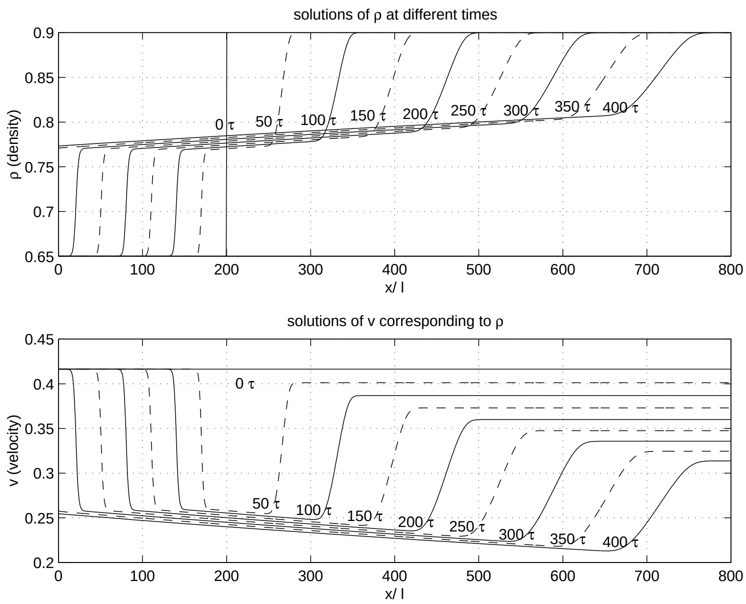

Figure 3.9: H1-R2 Solutions at Selected Times

vector $(e^{2N-N})_{i=1}^{N}$ between these two solutions as

$$\mathbf{e}_i^{2N-N} = \frac{1}{2}(U_{2i-1}^{2N} + U_{2i}^{2N}) - U_i^N, i = 1, \cdots, N. \tag{3.73}$$

Then the relative error between the two solutions is defined as the norm of the difference vector:

$$\epsilon^{2N-N} = \parallel \mathbf{e}^{2N-N} \parallel. \tag{3.74}$$

The convergence rate is defined as

$$r = \log_2(\frac{\epsilon^{2N-N}}{\epsilon^{4N-2N}}). \tag{3.75}$$

In (3.74), the norm can be L^1-, L^2- or L^∞-norm.

For N equal to 64, 128, 256, 512 and 1024, the relative errors and convergence rates for the first-order method are given in **Table** 3.1, and those for the second-order Godunov's method are computed and given in **Table** 3.2. For the first-order Godunov's method, the convergence rates related to L^1-norm errors are around 1, which is larger than that related to L^2-norm errors and even larger than that related L^∞-norm errors. From **Table** 3.1 we also see that the rates for ρ and v are consistent since ρ and v are in equilibrium at 400τ. In **Table** 3.2, the convergence rates for the second-order method, although better slightly than those for first-order method, are not second order due to the effect of the relaxation term.

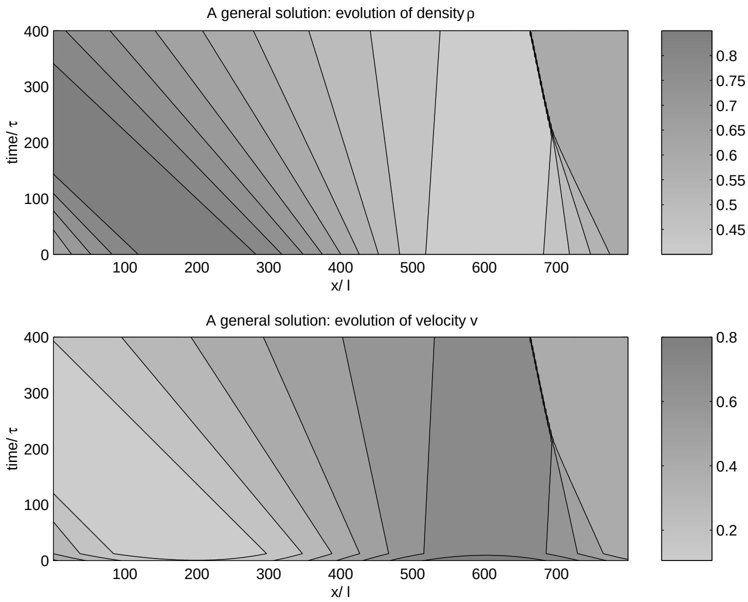

Figure 3.10: A General Solution of Zhang's Model with Neumann BC

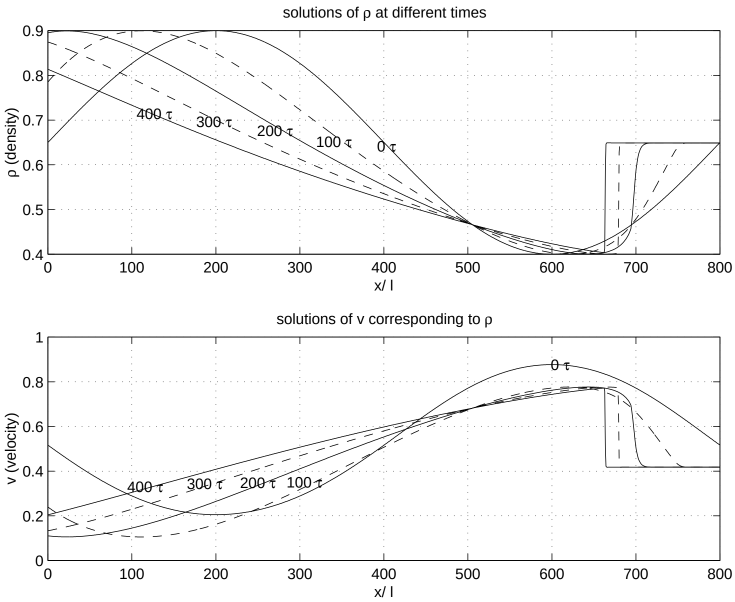

Figure 3.11: The Solutions from **Figure** 3.10 at Selected Times

ρ	128-64	Rate	256-128	Rate	512-256	Rate	1024-512
L^1	3.43e-03	0.969	1.75e-03	0.985	8.84e-04	0.994	4.44e-04
L^2	6.94e-03	0.632	4.48e-03	0.635	2.88e-03	0.718	1.75e-03
L^∞	4.56e-02	0.0219	4.49e-02	0.0973	4.20e-02	0.355	3.28e-02
v	128-64	Rate	256-128	Rate	512-256	Rate	1024-512
L^1	4.83e-03	0.973	2.46e-03	0.985	1.24e-03	0.991	6.25e-04
L^2	9.86e-03	0.631	6.37e-03	0.628	4.12e-03	0.695	2.54e-03
L^∞	6.53e-02	0.0243	6.42e-02	0.0903	6.03e-02	0.313	4.86e-02

Table 3.1: Convergence rates for the first-order method with initial conditions (3.71,3.72)

ρ	128-64	Rate	256-128	Rate	512-256	Rate	1024-512
L^1	5.81e-03	0.966	2.98e-03	1.03	1.46e-03	1.05	7.06e-04
L^2	9.85e-03	0.823	5.57e-03	0.836	3.12e-03	0.885	1.69e-03
L^∞	3.73e-02	0.215	3.22e-02	0.232	2.74e-02	0.616	1.79e-02
v	128-64	Rate	256-128	Rate	512-256	Rate	1024-512
L^1	8.24e-03	0.973	4.20e-03	1.03	2.05e-03	1.04	9.93e-04
L^2	1.40e-02	0.842	7.80e-03	0.865	4.28e-03	0.833	2.40e-03
L^∞	5.40e-02	0.250	4.54e-02	0.354	3.56e-02	0.527	2.47e-02

Table 3.2: Convergence rates for the second-order method with initial conditions (3.71)ini.2

Chapter 4

The PW Model and Its Numerical Solutions

4.1 Introduction

The Payne-Whitham (PW) model, suggested by Payne (1971) and Whitham (1974), is one of the first non-equilibrium traffic models. It can be written as

$$\begin{aligned} \rho_t + \rho v_x + v \rho_x &= 0 && (4.1) \\ v_t + v v_x + \frac{c_0^2}{\rho} \rho_x &= \frac{v_*(\rho) - v}{\tau}, && (4.2) \end{aligned}$$

where the traffic sound speed $c_0 > 0$ is constant, and $v_*(\rho)$ is the relationship between velocity v and density ρ for equilibrium states. The fundamental diagram $f_*(\rho) = \rho v_*(\rho)$, reflecting basic features of a roadway, is assumed to be known. Setting $m = \rho v$, (4.1) and (4.2) can be written as

$$\begin{pmatrix} \rho \\ m \end{pmatrix}_t + \begin{pmatrix} m \\ \frac{m^2}{\rho} + c_0^2 \rho \end{pmatrix}_x = \begin{pmatrix} 0 \\ \frac{f_*(\rho) - m}{\tau} \end{pmatrix}, \tag{4.3}$$

which is in conservative form

$$u_t + f(u)_x = s(u), \tag{4.4}$$

with state $u = (\rho, m)$ of traffic flow.

For $c_0 = \rho v_*'(\rho)$, system (4.3) becomes Zhang's model, which is discussed in Chapter 3. Both PW model and Zhang's model are "systems of hyperbolic conservation laws with relaxation" in the sense of Whitham (1959; 1974) and Liu (1987).

Schochet (1988) has shown that, as $\tau \to 0$, the system (4.3) admits the limit

$$\rho_t + (\rho v_*)_x = \nu \frac{\partial^2 \rho}{\partial x^2}. \tag{4.5}$$

Note that (4.5) is the LWR model with viscous right handside.

Generally, the equilibrium velocity is assumed to be decreasing with respect to density; i.e., ${v_*}'(\rho) < 0$; the equilibrium flow rate is concave; i.e., $f_*''(\rho) < 0$. Equation (4.3) has three different wave velocities (relative to the road): λ_*, λ_1 and λ_2. The first-order wave speed λ_* is

$$\lambda_*(\rho) = v_*(\rho) + \rho {v_*}'(\rho). \tag{4.6}$$

λ_* can be positive or negative. Since the wave speed of the degenerate system (i.e., the LWR model), it is called a sub-characteristic. The second-order wave speeds, or "frozen characteristic speeds" (Pember, 1993), are

$$\lambda_1(\rho, v) = v - c_0, \tag{4.7}$$

$$\lambda_2(\rho, v) = v + c_0. \tag{4.8}$$

Since $v, c_0 \geq 0$, $\lambda_1 < \lambda_2$ and $v + c_0 > 0$.

Whitham (1959; 1974) showed that the stability condition for the linearized system with a relaxation term is

$$\lambda_1 < \lambda_* < \lambda_2 \qquad \text{when } t = 0. \tag{4.9}$$

Liu (1987) showed that if condition (4.9) is always satisfied, then the corresponding LWR model is stable under small perturbations and the time-asymptotic solutions of the system (4.3) are completed determined by the equilibrium LWR model. Chen, Levermore, and Liu (1994) showed that if condition (4.9) is satisfied, then solutions of the system tend to solutions of the equilibrium equations as the relaxation time tends to zero. Besides (4.9), that $\lambda_1 \neq 0$ for all x and t can serve as another stability condition, since, otherwise, the standing wave $f(u)_x = s(u)$ may be singular and can't always be solved.

This chapter is organized as follows. After discussing the boundary averages in section 2, we study several different Godunov methods for the PW model in section 3. In section 4, we present numerical solutions to the PW model.

4.2 Computation of the boundary averages of ρ and v

To develop Godunov's methods for the PW model, we first partition a piece of roadway, e.g., an interval of $[a, b]$, into N zones, and then approximate current traffic conditions ρ and v with certain types of functions. At each zone boundary, the averages of ρ and v over time have to be computed at every time step for computing ρ and v at next time step.

For a system of conservation laws, we can compute the boundary averages by solving a Riemann problem, which has been discussed by Smoller (1983). For the homogeneous version of the PW model, we can adopt the solutions by Zhang (2000a). Zhang developed solutions to the Riemann problem for the homogeneous version of Zhang's model, which is similar to the PW model, and obtained 8 types of wave solutions and the formula for the boundary averages of ρ and v related to each type of solutions. However, the PW model has one relaxation term. The Riemann problem for (4.3) with a source term is still open. In this section, we still calculate the boundary averages based on the solutions to a Riemann problem for the homogeneous version of the PW model.

Liu (1979) discussed the Cauchy problem for a hyperbolic system of conservation laws with source terms. Inspired by his study, we present another approach of computing the boundary averages of ρ and v by solving a Cauchy problem for (4.3). This method is presented in the second part of this section.

4.2.1 Computing the boundary averages from the Riemann problem

In this subsection, we study the Riemann problem for the homogeneous version of (4.3) with the following jump initial conditions:

$$u_{i+1/2}(x, t=0) \;=\; \begin{cases} U_l, & \text{if } x < x_{i+1/2} \\ U_r, & \text{if } x \geq x_{i+1/2} \end{cases}, \tag{4.10}$$

where the left state $U_l = (\rho_l, v_l)$ and the right state $U_r = (\rho_r, v_r)$ are constant. For computational purpose, we are interested in the averages of ρ and v at the boundary $x = x_{i+1/2}$ over a time interval Δt, which are denoted by $\rho^{*j}_{i+1/2}$ and $v^{*j}_{i+1/2}$; i.e., we want to find

$$\rho^{*j}_{i+1/2} = \frac{1}{\Delta t}\int_0^{\Delta t} \rho(x=0,t)\mathrm{dt} \quad \text{and} \quad v^{*j}_{i+1/2} = \frac{1}{\Delta t}\int_0^{\Delta t} v(x=0,t)\mathrm{dt}. \tag{4.11}$$

For the homogeneous PW model, the equations of the characteristic curves are written in terms of (ρ, v) instead of (ρ, m), and the left and right initial values for v are given as $v_l = \frac{m_l}{\rho_l}$ and $v_r = \frac{m_r}{\rho_r}$. Thus the boundary average of m, $m^{*j}_{i+1/2} = \rho^{*j}_{i+1/2} v^{*j}_{i+1/2}$, can be easily obtained once we computed $\rho^{*j}_{i+1/2}$ and $v^{*j}_{i+1/2}$.

Determined by the relationship between left state (ρ_l, v_l) and right state (ρ_r, v_r), there are 8 types of wave solutions to the Riemann problem, including 4 first-order waves and 4 second-order waves. The four first-order wave solutions are a 1-shock, a 2-shock, a 1-rarefaction and a 2-rarefaction. The four second-order wave solutions are a H1-H2 (Left-Shock-Right-Shock) wave, a R1-R2 (Left-Rarefaction-Right-Rarefaction) wave, a R1-H2 (Left-Rarefaction-Right-Shock) wave and a H1-R2 (Left-Shock-Right-Rarefaction) wave.

In the remaining part of this subsection, we define the velocity flux function $\phi(\rho)$ as $\phi(\rho) = c_0^2\rho$, discuss the eight types of wave solutions to the Riemann problem one by one, and present a table containing the boundary averages $\rho^{*j}_{i+1/2}$ and $v^{*j}_{i+1/2}$ for each case.

1. The wave solution is a 1-shock if the left and right states satisfy

$$\text{H1: } v_r - v_l = -\sqrt{\frac{2(\rho_l - \rho_r)(\phi(\rho_l) - \phi(\rho_r))}{\rho_l \rho_r}}, \quad \rho_r > \rho_l,\ v_r < v_l. \tag{4.12}$$

The wave speed is

$$s = \frac{\rho_r v_r - \rho_l v_l}{\rho_r - \rho_l} \tag{4.13}$$

The solutions $(\rho^{*j}_{i+1/2}, v^{*j}_{i+1/2})$ for case 1 are summarized in the following table:

	$s = \frac{\rho_r v_r - \rho_l v_l}{\rho_r - \rho_l}$	$\rho^{*j}_{i+1/2}$	$v^{*j}_{i+1/2}$
H1	$s > 0$	ρ_l	v_l
	$s < 0$	ρ_r	v_r
	$s = 0$	$\frac{\rho_l+\rho_r}{2}$	$\frac{v_l+v_r}{2}$

2. The wave solution is a 2-shock if the left and right states satisfy

$$\text{H2: } v_r - v_l = -\sqrt{\frac{2(\rho_l - \rho_r)(\phi(\rho_l) - \phi(\rho_r))}{\rho_l \rho_r}} \quad \rho_r < \rho_l,\ v_r < v_l \tag{4.14}$$

The wave speed is

$$s = \frac{\rho_r v_r - \rho_l v_l}{\rho_r - \rho_l} > 0 \tag{4.15}$$

The solutions $(\rho^{*j}_{i+1/2}, v^{*j}_{i+1/2})$ for case 2 are summarized in the following table:

	$s = \frac{\rho_r v_r - \rho_l v_l}{\rho_r - \rho_l}$	$\rho^{*j}_{i+1/2}$	$v^{*j}_{i+1/2}$
H2	$s > 0$	ρ_l	v_l

3. The wave solution is a 1-rarefaction if the left and right states satisfy

$$\text{R1: } v_r - v_l = v_*(\rho_r) - v_*(\rho_l) \quad \rho_r < \rho_l,\ v_r > v_l \tag{4.16}$$

The characteristic velocity is determined by the first eigenvalue of the system:

$$\lambda_1(\rho, v) = v - c_0. \tag{4.17}$$

If $\lambda_1(\rho_l, v_l) > 0$, the boundary averages $\rho^{*j}_{i+1/2}$ and $v^{*j}_{i+1/2}$ are the left initial values for ρ and v , similarly, if $\lambda_1(\rho_r, v_r) < 0$, they are the right initial values. Otherwise, $(\rho^{*j}_{i+1/2}, v^{*j}_{i+1/2})$ are solutions to the equations:

$$\lambda_1(\rho^{*j}_{i+1/2}, v^{*j}_{i+1/2}) = v^{*j}_{i+1/2} - c_0 = 0, \tag{4.18}$$

$$v^{*j}_{i+1/2} - v_l = v_*(\rho^{*j}_{i+1/2}) - v_*(\rho_l), \tag{4.19}$$

which can be simplified as follows,

$$v^{*j}_{i+1/2} = c_0, \tag{4.20}$$

$$v_*(\rho^{*j}_{i+1/2}) = c_0 - v_l + v_*(\rho_l). \tag{4.21}$$

The solutions $(\rho^{*j}_{i+1/2}, v^{*j}_{i+1/2})$ to (4.20,4.21) for case 3 are summarized in the following table:

	λ_1	$\rho^{*j}_{i+1/2}$	$v^{*j}_{i+1/2}$
R1	$\lambda_1(\rho_l, v_l) > 0$	ρ_l	v_l
	$\lambda_1(\rho_r, v_r) < 0$	ρ_r	v_r
	o.w.	solution to equations 4.20, 4.21	

4. The wave solution is a 2-rarefaction if the left and right states satisfy

$$\text{R2: } v_r - v_l = v_*(\rho_l) - v_*(\rho_r) \quad \rho_r > \rho_l,\ v_r > v_l \tag{4.22}$$

The characteristic velocity is the second eigenvalue of the system:

$$\lambda_2(\rho, v) = v + c_0 > 0. \tag{4.23}$$

The solutions $(\rho^{*j}_{i+1/2}, v^{*j}_{i+1/2})$ for case 4 are summarized in the following table:

	λ_2	$\rho^{*j}_{i+1/2}$	$v^{*j}_{i+1/2}$
R2	$\lambda_2 > 0$	ρ_l	v_l

5. The wave solution is a 1-rarefaction + 2-rarefaction with an intermediate state (ρ_m, v_m) if the left, right and intermediate states satisfy

$$\text{R1: } v_m - v_l = v_*(\rho_m) - v_*(\rho_l) \quad \rho_m < \rho_l,\ v_m > v_l; \tag{4.24}$$

$$\text{R2: } v_r - v_m = v_*(\rho_m) - v_*(\rho_r) \quad \rho_r > \rho_m,\ v_r > v_m. \tag{4.25}$$

Adding (4.24) to (4.25) we find

$$2 * v_*(\rho_m) - v_*(\rho_l) - v_*(\rho_r) - (v_r - v_l) = 0, \tag{4.26}$$

for $\rho_m < \rho_l, \rho_m < \rho_r$. Thus

$$v_m = v_*(\rho_m) + v_l - v_*(\rho_l). \tag{4.27}$$

The solutions $(\rho^{*j}_{i+1/2}, v^{*j}_{i+1/2})$ for case 5 are summarized in the following table:

	λ_1	$\rho^{*j}_{i+1/2}$	$v^{*j}_{i+1/2}$
	$\lambda_1(\rho_l, v_l) > 0$	ρ_l	v_l
R1-R2	$\lambda_1(\rho_m, v_m) < 0$	ρ_m	v_m
	o.w.	solution to equations 4.20, 4.21	

6. The wave solution is a 1-rarefaction + 2-shock with an intermediate state (ρ_m, v_m) if the left, right and intermediate states satisfy

$$\text{R1: } v_m - v_l = v_*(\rho_m) - v_*(\rho_l), \quad \rho_m < \rho_l,\ v_m > v_l \tag{4.28}$$

$$\text{H2: } v_r - v_m = -\sqrt{\frac{2(\rho_m - \rho_r)(\phi(\rho_m) - \phi(\rho_r))}{\rho_m \rho_r}}, \quad \rho_r < \rho_m,\ v_r < v_m. \tag{4.29}$$

These two equations yield

$$v_*(\rho_m) - v_*(\rho_l) - \sqrt{\tfrac{2(\rho_m-\rho_r)(\phi(\rho_m)-\phi(\rho_r))}{\rho_m\rho_r}} - (v_r - v_l) \ = 0, \qquad (4.30)$$

for $\rho_r < \rho_m < \rho_l$. Thus

$$v_m = v_*(\rho_m) + v_l - v_*(\rho_l). \qquad (4.31)$$

The solutions $(\rho^{*j}_{i+1/2}, v^{*j}_{i+1/2})$ for case 6 are summarized in the following table:

	λ_1	$\rho^{*j}_{i+1/2}$	$v^{*j}_{i+1/2}$
R1-H2	$\lambda_1(\rho_l, v_l) > 0$	ρ_l	v_l
	$\lambda_1(\rho_m, v_m) < 0$	ρ_m	v_m
	o.w.	solution to equations 4.20, 4.21	

7. The wave solution is a 1-shock + 2-shock with an intermediate state (ρ_m, v_m) if the left, right and intermediate states satisfy

$$\text{H1: } v_m - v_l = -\sqrt{\tfrac{2(\rho_l-\rho_m)(\phi(\rho_l)-\phi(\rho_m))}{\rho_l\rho_m}}, \quad \rho_m > \rho_l,\ v_m < v_l; \qquad (4.32)$$

$$\text{H2: } v_r - v_m = -\sqrt{\tfrac{2(\rho_m-\rho_r)(\phi(\rho_m)-\phi(\rho_r))}{\rho_m\rho_r}}, \quad \rho_r < \rho_m,\ v_r < v_m. \qquad (4.33)$$

These two equations imply

$$\sqrt{\frac{2(\rho_l-\rho_m)(\phi(\rho_l)-\phi(\rho_m))}{\rho_l\rho_m}} + \sqrt{\frac{2(\rho_m-\rho_r)(\phi(\rho_m)-\phi(\rho_r))}{\rho_m\rho_r}} + (v_r - v_l) \ = \ 0, \qquad (4.34)$$

for $\rho_m > \rho_l, \rho_m > \rho_r$. Thus

$$v_m = -\sqrt{\frac{2(\rho_l-\rho_m)(\phi(\rho_l)-\phi(\rho_m))}{\rho_l\rho_m}} + v_l. \qquad (4.35)$$

The solutions $(\rho^{*j}_{i+1/2}, v^{*j}_{i+1/2})$ for case 7 are summarized in the following table:

	$s = \frac{\rho_m v_m - \rho_l v_l}{\rho_r - \rho_l}$	$\rho^{*j}_{i+1/2}$	$v^{*j}_{i+1/2}$
H1-H2	$s > 0$	ρ_l	v_l
	$s < 0$	ρ_m	v_m
	$s = 0$	$\frac{\rho_l+\rho_m}{2}$	$\frac{v_l+v_m}{2}$

8. The wave solution is a 1-shock + 2-rarefaction with an intermediate state (ρ_m, v_m) if the left, right and intermediate states satisfy

$$\text{H1: } v_m - v_l = -\sqrt{\tfrac{2(\rho_l-\rho_m)(\phi(\rho_l)-\phi(\rho_m))}{\rho_l\rho_m}}, \quad \rho_m > \rho_l,\ v_m < v_l; \tag{4.36}$$

$$\text{R2: } v_r - v_m = v_*(\rho_m) - v_*(\rho_r), \quad \rho_r > \rho_m,\ v_r > v_m. \tag{4.37}$$

These two equations imply

$$-\sqrt{\tfrac{2(\rho_l-\rho_m)(\phi(\rho_l)-\phi(\rho_m))}{\rho_l\rho_m}} + v_*(\rho_m) - v_*(\rho_r) - (v_r - v_l) = 0 \tag{4.38}$$

for $\rho_m > \rho_l, \rho_m > \rho_r$. Thus

$$v_m = -\sqrt{\frac{2(\rho_l-\rho_m)(\phi(\rho_l)-\phi(\rho_m))}{\rho_l\rho_m}} + v_l. \tag{4.39}$$

The solutions $(\rho^{*j}_{i+1/2}, v^{*j}_{i+1/2})$ for case 8 are summarized in the following table:

	$s = \frac{\rho_m v_m - \rho_l v_l}{\rho_r - \rho_l}$	$\rho^{*j}_{i+1/2}$	$v^{*j}_{i+1/2}$
H1-R2	$s > 0$	ρ_l	v_l
	$s < 0$	ρ_m	v_m
	$s = 0$	$\frac{\rho_l+\rho_m}{2}$	$\frac{v_l+v_m}{2}$

4.2.2 Computing the boundary averages from the Cauchy problem

Liu (1979) studied the Cauchy problem for a hyperbolic system of conservation laws with source terms. In this subsection we apply his theory to find the boundary averages by solving the Cauchy problem for the PW model.

The homogeneous version of the PW model can be written as follows,

$$u_t + f(u)_x = 0, \tag{4.40}$$

where $u = (\rho, v)$. The Riemann problem for this system at $x = 0$ has the following initial conditions:

$$u(x, t_j) = \begin{cases} U_l, & \text{if } x < 0 \\ U_r, & \text{if } x > 0 \end{cases}. \tag{4.41}$$

The wave solutions to the Riemann problem consist of two basic waves with an intermediate state U_1. By denoting $U_0 \equiv U_l$ and $U_2 \equiv U_r$, we define (U_{i-1}, U_i) as the $i^{th}(i = 1, 2)$ propagation wave. Each basic wave (U_{i-1}, U_i) may be a shock or a rarefaction. These wave solutions, which have been discussed in previous subsection, serve as the basis for solutions to a related Cauchy problem.

The Cauchy problem for the PW model has the following initial conditions:

$$u(x, t_j) = \begin{cases} u_l(x), & \text{if } x < 0 \\ u_r(x), & \text{if } x > 0 \end{cases}, \tag{4.42}$$

in which,

$$f(u_l(x))_x = s(u_l(x)), \qquad u_l(0) = U_l \tag{4.43}$$

$$f(u_r(x))_x = s(u_r(x)), \qquad u_r(0) = U_r. \tag{4.44}$$

Here the intermediate state $u_1(x)$ is determined from

$$f(u_1(x))_x = s(u_1(x)), \qquad u_1(0) = U_1, \tag{4.45}$$

in which U_1 is the intermediate state solution to the corresponding Riemann problem. We denote $u_0(x) \equiv u_l(x)$ and $u_2(x) \equiv u_r(x)$, and define $(u_{i-1}(x), u_i(x))$ as the $i^{th}(i = 1, 2)$ propagation wave of the Cauchy problem.

For computational purposes, we still want to compute the boundary average of $u(x, t)$ at $x = 0$; i.e., $U^* \equiv \int_0^{\Delta t} u(0, t)dt$. The boundary average varies when $x = 0$ is covered by different states or waves. Since solutions to the Cauchy problem for the PW model consist of three states and four types of waves, the boundary $x = 0$ may be covered by the left, right or intermediate state, and may be crossed by 1-shock, 2-shock, 1-rarefaction or 2-rarefaction wave.

If the boundary $x = 0$ is covered by the intermediate state, according to the definition of the intermediate state, the solutions of the boundary average U^* is equal to U_1. Similarly, $U^* = U_l$ or U_r when the boundary is covered by the left or right state.

Of the 4 types of basic waves, the 2-H and 2-R waves never cross $x = 0$ since $\lambda_2(U) > 0$, and 1-shock still propagates along a line described by $\frac{x}{t} = \sigma(U_{i-1}, U_i)$. Therefore, these three waves don't affect the boundary averages. In the remaining part, we consider the adjustment to the 1-rarefaction wave.

The 1-rarefaction wave was shown by Liu to be a perturbation on the solutions to the corresponding Riemann problem. Assume that $(u_{i-1}(x), u_i(x))$ is a 1-R wave, $u_{i-1}(x)$ and $u_i(x)$ are separated in a region $x_{i-1}(t) < x < x_i(t)$. The wave solution of the Cauchy problem (4.42) approaches the 1-rarefaction wave (U_{i-1}, U_i) as $t \to 0$,

$$\begin{cases} \lim_{t\to 0} \frac{x_{i-1}(t)}{t} = \lambda_1(u_{i-1}(x)) \equiv \xi_0 \\ \lim_{t\to 0} \frac{x_i(t)}{t} = \lambda_1(u_i(x)) \equiv \xi_1 \end{cases} \tag{4.46}$$

$$\lim_{t\to 0; \frac{x}{t}=\eta} u(x,t) = v(\eta), \quad x_{i-1}(t) < x < x_i(t), \tag{4.47}$$

where $v(\eta) \in R_1(U_{i-1})$ with $\lambda_1(v(\eta)) = \eta$.

Using the coordinate of time t, we define the initial i-characterized speed ξ as follows:

$$\frac{\partial x(\xi,t)}{\partial t} = \lambda_1(w(\xi,t)) \tag{4.48}$$

$$w(\xi,t) = u(x(\xi,t),t) \tag{4.49}$$

and

$$w(\xi,0) = v(\xi) \equiv \phi(\xi) \tag{4.50}$$

$$x_{i-1} = x(\xi_0, t) \tag{4.51}$$

$$u(x(\xi_0, t), t) = u_{i-1}(x(\xi_0, t), t) = u_{i-1}(x(\xi_0, t)) \tag{4.52}$$

$$u(x(\xi_1, t), t) = u_i(x(\xi_1, t), t) = u_i(x(\xi_1, t)) \tag{4.53}$$

For a homogeneous system ξ will be a constant slope for characteristics. However, ξ is not constant for the PW model with a source term.

With the transformation (4.48,4.49), the original system

$$\frac{\partial u(x(\xi, t), t)}{\partial t} + A(u)\frac{\partial u}{\partial x} = s(u) \qquad \text{in which } A(u) = \nabla f(u) \tag{4.54}$$

becomes

$$\begin{aligned} \frac{\partial x(\xi, t)}{\partial t} &= \lambda_1(w(\xi, t)) && (4.55)\\ \frac{\partial x}{\partial \xi}\frac{\partial w}{\partial t} + (A - \lambda_1)\frac{\partial w}{\partial \xi} &= \frac{\partial x}{\partial \xi} s. && (4.56) \end{aligned}$$

Since

$$x(\xi, 0) = 0, \tag{4.57}$$

we obtain

$$\begin{aligned} x(\xi, t) &= \frac{\partial x}{\partial t}|_{t=0} t + \frac{1}{2}\frac{\partial^2 x}{\partial t^2}|_{t=0} t^2 + \mathbf{O}(t^3) \\ &= \xi t + \frac{1}{2}\frac{\partial^2 x}{\partial t^2}|_{t=0} t^2 + \mathbf{O}(t^3) && (4.58) \end{aligned}$$

We calculate $\frac{\partial^2 x}{\partial t^2}$ as follows:

$$\begin{aligned} \frac{\partial^2 x}{\partial t^2} &= \frac{\partial \lambda_1(w)}{\partial t} = \nabla\lambda_1 \frac{\partial w}{\partial t} \\ &= \nabla\lambda_1 (\frac{\partial u}{\partial x}\frac{\partial x}{\partial t} + \frac{\partial u}{\partial t}) = \nabla\lambda_1 (s + (\xi I - A)\frac{\partial u}{\partial x})|_{t=0} \\ &= \nabla\lambda_1 s + \mathbf{O}(t), && (4.59) \end{aligned}$$

where we assume the difference between $\xi\frac{\partial u}{\partial x}$ and $A\frac{\partial u}{\partial x}$ is small since $-\xi u_\xi + f(u)_\xi = 0$ for a rarefaction wave. Then, the rarefaction wave path is

$$x(t) = \lambda_1 t + \frac{1}{2}\nabla\lambda_1(u)s(u)t^2 + \mathbf{O}(t^3)$$

$$= \quad (\frac{m}{\rho} - c_0)t + \frac{f_* - m}{2\tau\rho}t^2 + \mathbf{O}(t^3). \qquad (4.60)$$

which is a parabola. The linear term of the rarefaction wave is the 1-R wave for the Riemann problem. The second-order term is determined by the source term. For small time scales; i.e., t small, this rarefaction wave is a perturbation of the rarefaction for the corresponding Riemann problem. The 2-rarefaction wave functions can be derived similarly, although they are not necessary for computing the boundary averages.

Recall that, by assumption, the characteristic curve of 1-rarefaction wave is

$$v_l \quad = \quad v_*(\rho) - v_*(\rho_l). \qquad (4.61)$$

Let $x(t) = 0$. From (4.60) we get

$$v \quad = \quad c_0 - \frac{f_* - m}{2\tau\rho}t \qquad (4.62)$$

$$\rho \quad = \quad v_*^{-1}(v - v_l + v_*(\rho_l)) = v_*^{-1}(\rho_0) - \frac{1}{v_*'(\rho_0)}\frac{f_* - m}{2\tau\rho}t, \qquad (4.63)$$

from which we can calculate $U^* \equiv \int_0^{\Delta t} u(0,t)dt$.

The above analysis shows that the 1-rarefaction wave fans of the Cauchy problem consists of parabolic curves instead of lines. When we use these parabolic rarefaction waves to compute U^*, the numerical solution of the PW model improves. However, the adjustment for a 1-rarefaction wave is needed only when it crosses the boundary $x = 0$, and 1-rarefaction waves are adjusted with a lower order perturbation in a short time step Δt. Thus this improvement doesn't appear to be significant. Besides, we have $\lambda_1(U) = 0$ for some state U when 1-rarefaction wave cross the boundary. Therefore, the state U is in the unstable region for the PW model. This may be another reason that this adjustment doesn't yield significantly better solutions.

4.3 Godunov methods

In this section, we study Godunov methods for solving the PW model (4.3). For a general system (4.4), the finite difference equations are

$$U_i^{j+1} = U_i^j - \frac{\Delta t}{\Delta x}(f(U_{i+1/2}^{j+1/2}) - f(U_{i-1/2}^{j+1/2})) + \Delta t \tilde{s}(U), \tag{4.64}$$

in which U_i^{j+1} U_i^j are both averages of $u(x,t)$ over i^{th} cell at time $(j+1)\Delta t$ and $j\Delta t$, $U_{i\pm 1/2}^{j+1/2}$ are the boundary averages calculated as shown in the preceding section, and $\tilde{s}(U)$ is the source average over $((i-1/2)\Delta x, (i+1/2)\Delta x) \times (j\Delta t, (j+1)\Delta t)$.

When we treat the source term implicitly, the system is discretized as

$$\frac{\rho_i^{j+1} - \rho_i^j}{k} + \frac{m_{i+1/2}^{*j} - m_{i-1/2}^{*j}}{h} = 0 \tag{4.65}$$

$$\frac{m_i^{j+1} - m_i^j}{k} + \frac{\frac{{m_{i+1/2}^{*j}}^2}{\rho_{i+1/2}^{*j}} + c_0^2 \rho_{i+1/2}^{*j} - \frac{{m_{i-1/2}^{*j}}^2}{\rho_{i-1/2}^{*j}} - c_0^2 \rho_{i-1/2}^{*j}}{h} = \frac{f_*(\rho_i^{j+1}) - m_i^{j+1}}{\tau} \tag{4.66}$$

in which, ρ_i^j and m_i^j are the cell average of ρ and m respectively over the ith cell, and $\rho_{i+1/2}^{*j}$ and $m_{i+1/2}^{*j}$ are the averages of ρ and m respectively on the cell boundary $x_{i+1/2}$ in the time interval (t_j, t_{j+1}). In (4.66), the source term $\tilde{s}(U)$ is treated implicitly.

From (4.65,4.66), we can write the evolution equations for the PW model as

$$\rho_i^{j+1} = \rho_i^j - \frac{k}{h}(m_{i+1/2}^{*j} - m_{i-1/2}^{*j}) \tag{4.67}$$

$$m_i^{j+1} = \frac{1}{(1+\frac{k}{\tau})}\{m_i^j - \frac{k}{h}[\frac{{m_{i+1/2}^{*j}}^2}{\rho_{i+1/2}^{*j}} + c_0^2 \rho_{i+1/2}^{*j} - \frac{(m_{i-1/2}^{*j})^2}{\rho_{i+1/2}^{*j}} - c_0^2 \rho_{i-1/2}^{*j}] + \frac{k}{\tau} f_*(\rho_i^{j+1})\} \tag{4.68}$$

In a first-order Godunov method we use the cell averages $\rho_l = \rho_i^j, m_l = m_i^j$ and $\rho_r = \rho_{i+1}^j, m_r = m_{i+1}^j$ as left/right states as the initial condition for the Riemann problem

$$u_{i+1/2}(x,t_j) = \begin{cases} U_l, & \text{if } x - x_{i+1/2} < 0 \\ U_r, & \text{if } x - x_{i+1/2} \geq 0 \end{cases}. \tag{4.69}$$

4.3.1 The Second-order Godunov Method

In this subsection we introduce a second-order Godunov method for the PW model in the process similar to that in section 3.3.

We begin by writing the PW model in the linearized form

$$u_t + A(u)u_x \ = \ s(u), \tag{4.70}$$

where

$$u \ = \ \begin{pmatrix} \rho(x,t) \\ m(x,t) \end{pmatrix} \tag{4.71}$$

and

$$A(u) \ = \ \begin{pmatrix} 0 & 1 \\ -\frac{m^2}{\rho^2} + c_0^2 & \frac{2m}{\rho} \end{pmatrix}. \tag{4.72}$$

The eigenvalues and eigenvectors of $A(u)$ are

$$\begin{aligned} \lambda_1(u) &= \tfrac{m}{\rho} - c_0, \quad r_1(u) = [1, \lambda_1]^t = [1, \tfrac{m}{\rho} - c_0]^t \\ \lambda_2(u) &= \tfrac{m}{\rho} + c_0, \quad r_1(u) = [1, \lambda_2]^t = [1, \tfrac{m}{\rho} + c_0]^t \end{aligned} \tag{4.73}$$

We diagonalize $A(u)$ by

$$T^{-1}(u)A(u)T(u) \ = \ \begin{pmatrix} \lambda_1(u) & 0 \\ 0 & \lambda_2(u) \end{pmatrix} \equiv \Lambda(u), \tag{4.74}$$

where the transformation matrix $T(u)$ is

$$T(u) \ = \ \begin{pmatrix} 1 & 1 \\ \frac{m}{\rho} - c_0 & \frac{m}{\rho} + c_0 \end{pmatrix}. \tag{4.75}$$

Letting $W = T^{-1}(u)u$, the PW model under the transformation becomes

$$W_t + \Lambda(u)W_x \;=\; T^{-1}(u)s(u). \tag{4.76}$$

Therefore, the PW model is transformed into two separated scalar equations in $W = (w_1, w_2)$. For the scalar equation in w_i ($i = 1, 2$), we introduce an interpolation for $w_i(x,t)$ which yields a second-order Godunov method for solving this equation. In the remaining part of this subsection, we first introduce an interpolation for $w_i(x,t)$ and then apply inverse transformation on them in order to develop a second-order method for the whole system.

For a scalar equation $w_t + \lambda(w)w_x = 0$, in a first-order Godunov method we use a step function $u_I(x,t_j)$ to interpolate the data at time t_j,

$$w_I(x,t_j) \;=\; w_i^j, \text{ if } x_{i-1/2} < x \leq x_{i+1/2}, \tag{4.77}$$

and solve the Riemann problem with the following initial conditions:

$$\begin{aligned} w_{i+1/2}^{j,L} &= w_i^j \\ w_{i-1/2}^{j,R} &= w_i^j \end{aligned} \tag{4.78}$$

In a second-order Godunov method, we interpolate the data at time t_j with a piecewise linear function,

$$w_I(x,t_j) \;=\; w_i^j + \frac{(x-ih)}{h}\Delta^{VL}w_i^j, \text{ if } x_{i-1/2} < x \leq x_{i+1/2}. \tag{4.79}$$

With a half-step prediction , the Riemann problem has the initial conditions of

$$\begin{aligned} w_{i+1/2}^{j+1/2,L} &= w_i^j + \tfrac{1}{2}(1-\lambda(w_i^j)\tfrac{k}{h})\Delta^{VL}w_i^j \\ w_{i-1/2}^{j+1/2,R} &= w_i^j - \tfrac{1}{2}(1+\lambda(w_i^j)\tfrac{k}{h})\Delta^{VL}w_i^j \end{aligned}\ , \tag{4.80}$$

where $\Delta^{VL}w_i^j$ is the van Leer slope (all superscripts j are suppressed)

$$\Delta^{VL}w_i \;=\begin{cases} S_i \cdot \min(2|w_{i+1}-w_i|, 2|w_i-w_{i-1}|, \frac{1}{2}|w_{i+1}-w_{i-1}|), & \varphi > 0 \\ 0, & \text{otherwise} \end{cases}$$

$$S_i = \mathrm{sign}(w_{i+1} - w_{i-1}) \tag{4.81}$$

$$\varphi = (w_{i+1} - w_i) \cdot (w_i - w_{i-1}) \tag{4.82}$$

We apply the above procedure twice to compute the half-step values $W_{i+1/2}^{j+1/2,L}$ and $W_{i-1/2}^{j+1/2,R}$. Then we apply the inverse transformation on these half-step values to obtain $U_{i+1/2}^{j+1/2,L}$ and $U_{i-1/2}^{j+1/2,R}$:

$$\begin{aligned} U_{i+1/2}^{j+1/2,L} &= T(U_i^j)W_{i+1/2}^{j+1/2,L} \\ U_{i-1/2}^{j+1/2,R} &= T(U_i^j)W_{i-1/2}^{j+1/2,R} \end{aligned} \tag{4.83}$$

With this new interpolation of ρ and m, we can solve the Riemann problem or the Cauchy problem on a cell boundary. For the inhomogeneous system, this second-order method has a convergence rate of 2. However, it is different for the PW model with a relaxation term.

4.3.2 Some other Godunov-type variant methods

In this subsection, we review other variants of Godunov method for (4.3) with a source term.

The first variant was suggested by Pember (1993a,1993b). He treated the source term as $\tilde{s}(U) = \frac{1}{2}(s(U_{i-1/2}^{j+1/2}) + s(U_{i+1/2}^{j+1/2}))$, where both $U_{i-1/2}^{j+1/2}$ and $U_{i+1/2}^{j+1/2}$ are the boundary averages solved in the Riemann problem.

The second variant is the fractional step splitting method, in which each time step Δt is split in-to three steps. In the first and third fractional steps, a first-order implicit method is used to integrate

$$\begin{pmatrix} \rho \\ m \end{pmatrix}_t = \begin{pmatrix} 0 \\ \frac{f_*(\rho)-m}{\tau} \end{pmatrix} \tag{4.84}$$

for time steps of $\Delta t/2$. In the second step, we solve the corresponding homogeneous system of (4.3), i.e.,

$$\begin{pmatrix} \rho \\ m \end{pmatrix}_t + \begin{pmatrix} m \\ \frac{m^2}{\rho} + c_0^2\rho \end{pmatrix}_x = 0 \tag{4.85}$$

for a time step of Δt.

A third variant is the quasi-steady wave-propagation algorithm suggested by LeVeque (1998a,1998b). This method introduces a new discontinuity in the center of each grid, i.e.,

$$\frac{1}{2}(U_i^- + U_i^+) \quad = \quad U_i, \tag{4.86}$$

and

$$f(U_i^+) - f(U_i^-) \quad = \quad s(U_i)\Delta x, \tag{4.87}$$

where $U_i^\pm = \begin{pmatrix} \rho_i^\pm \\ m_i^\pm \end{pmatrix}$. Then we get

$$\begin{pmatrix} m_i^+ - m_i^- \\ {m_i^+}^2/\rho_i^+ + c_0^2\rho_i^+ - {m_i^-}^2/\rho_i^- - c_0^2\rho_i^- \end{pmatrix} \quad = \quad \begin{pmatrix} 0 \\ \frac{f_*(\rho_i)-m_i}{\tau} \end{pmatrix}\Delta x \tag{4.88}$$

so $m_i^+ = m_i^- = m_i$. Setting

$$\rho_i^+ = \rho_i + \delta, \qquad \rho_i^- = \rho_i - \delta \tag{4.89}$$

we find

$$2c_0^2\delta^3 - K\delta^2 - (2m_i^2 + 2c_0^2\rho_i^2)\delta + K\rho_i^2 = 0, \tag{4.90}$$

in which $K = \frac{f_*(\rho_i)-m_i}{\tau}\Delta x$.

Given the solution to (4.90), LeVeque solved the Riemann problem of the homogeneous system with the initial conditions

$$u_{i+1/2}(x, t_j) \quad = \quad \begin{cases} U_i^+ & \text{if } x - x_{i+1/2} < 0 \\ U_i^- & \text{if } x - x_{i+1/2} \geq 0 \end{cases} \tag{4.91}$$

Then in the evolution equations, the source term is not considered.

In LeVeque's method, the data at time t_j are interpolated with a solution to the standing wave for the PW model in each cell. This method may be used together with the Cauchy problem we discussed before.

4.4 Numerical Solutions to the PW Model

In this section, we use the model parameters given in (Kerner, 1994), i.e., $c_0 = 2.48445 l/\tau$, $v_*(\rho) \equiv V(\rho) = 5.0461[(1+\exp\{[\rho - 0.25]/0.06\})^{-1} - 3.72 \times 10^{-6}] l/\tau$ and $L = 800l$. Here l is the unit of length, τ is the relaxation coefficient, and the section of the roadway is from $0l$ to $800l$. We set $l = 10$ (m) $\tau = 10$ (sec) and $\rho_h = 0.172$. The equilibrium functions $v_*(\rho)$ and $f_*(\rho)$ are given in **Figure** 4.1. In the figure, ρ_{c1}, ρ_{c2} are two critical densities and the region $\rho_{c1} < \rho < \rho_{c2}$ is the unstable region. According to (4.9), ρ_{c1} and ρ_{c2} satisfy the equation:

$$\rho v_*'(\rho) + c_0 \quad = \quad 0. \tag{4.92}$$

From this equation we get $\rho_{c1} = 0.173$,$\rho_{c2} = 0.396$.

For numerical computation purpose, we use two initial conditions:

$$\rho(x,0) \quad = \quad \rho_h + 0.02 \sin(2\pi x/800/l) \tag{4.93}$$

$$v(x,0) \quad = \quad v_*(\rho_h) - 0.02 \cos(2\pi x/800/l), \tag{4.94}$$

which is a global perturbation, and

$$\rho(x,0) \quad = \quad \begin{cases} \rho_h + \delta & \text{when } x \in [37.5l, 48.4l] \\ \rho_h - \delta/3 & \text{when } x \in [50.0l, 82.8l] \\ \rho_h & \text{otherwise} \end{cases} \tag{4.95}$$

$$v(x,0) \quad = \quad v_*(\rho(x,0)), \tag{4.96}$$

which is a local perturbation. Setting $\delta = 0.02$ and $\rho_h = 0.16$, the two initial conditions are given in **Figure** 4.2. The global perturbation is not in equilibrium, however the local perturbation is in equilibrium.

4.4.1 Stability test

The PW model is unstable in some regions, which is different from Zhang's model. In this subsection we test the stability property of the PW model at time $T_0 = 200.0\tau$. We use a first-order Godunov's method to compute the relative differences, defined in (3.73), between solutions with $N = 512$ grids and those with 1024 grids, and the difference between solutions with 1024 grids and those with 2048 grids. These differences are drawn as curves labeled as $1024 - 512$ and $2048 - 1024$ respectively in the following figures. Since the solutions (ρ, v) are close to the equilibrium state, only the differences of ρ are given. Given the convergent Godunov's method, the difference caused by different grid numbers decreases if the PW model is stable. We test the PW model with different initial conditions and different boundary conditions, which are in the stable or unstable region for the PW model, and the results are the same as predicted.

Setting $\rho_h = 0.16$ or $\rho_h = 0.17$ for the initial conditions (4.93,4.94), we solve the PW model with 512, 1024 and 2048 grids with periodic boundary conditions. The differences are shown in **Figure** 4.3. In the figure, the difference decreases when we increase the number of grids when $\rho_h = 0.16$; but the difference increases when $\rho_h = 0.17$. The figure proves that the PW model is stable for $\rho_h = 0.16$, and unstable for $\rho_h = 0.17$.

Using the same initial conditions as in last example, we solve the PW model with Neumann boundary conditions. The relative differences are given in **Figure** 4.4. In this case we get the same results as in last example.

Next we use the initial conditions (4.95,4.96) with $\delta = 0.02$. We solve the PW model with periodic boundary conditions. According to the differences shown in **Figure** 4.5, we conclude that the PW model also stable when $\rho_h = 0.16$ and unsta-

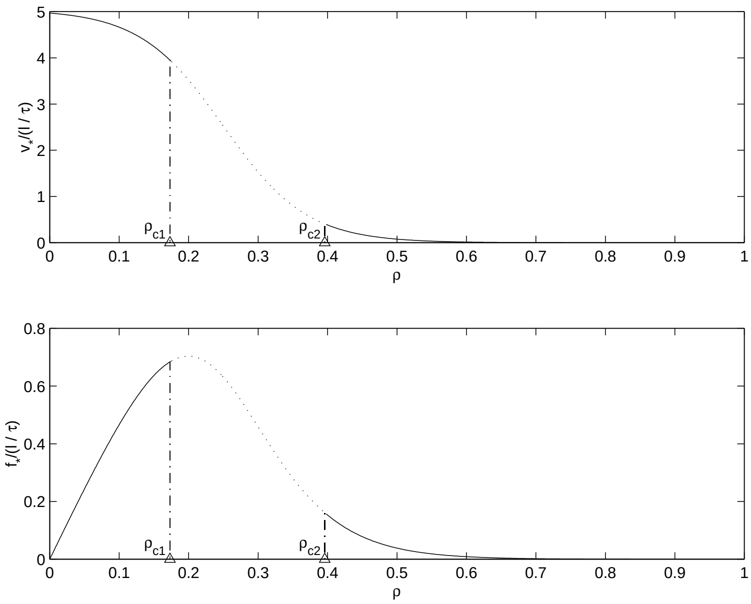

Figure 4.1: One selection of the equilibrium velocity and flow rate

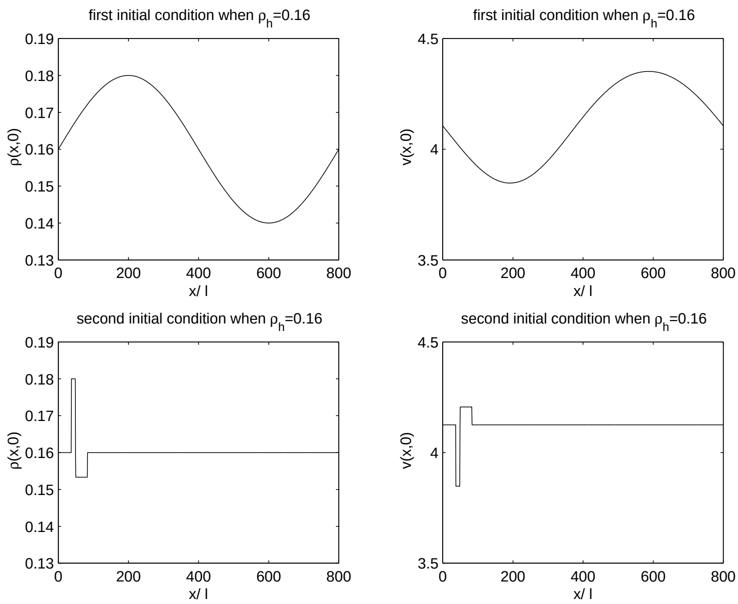

Figure 4.2: Two initial conditions: global non-equilibrium perturbation v.s. local equilibrium perturbation

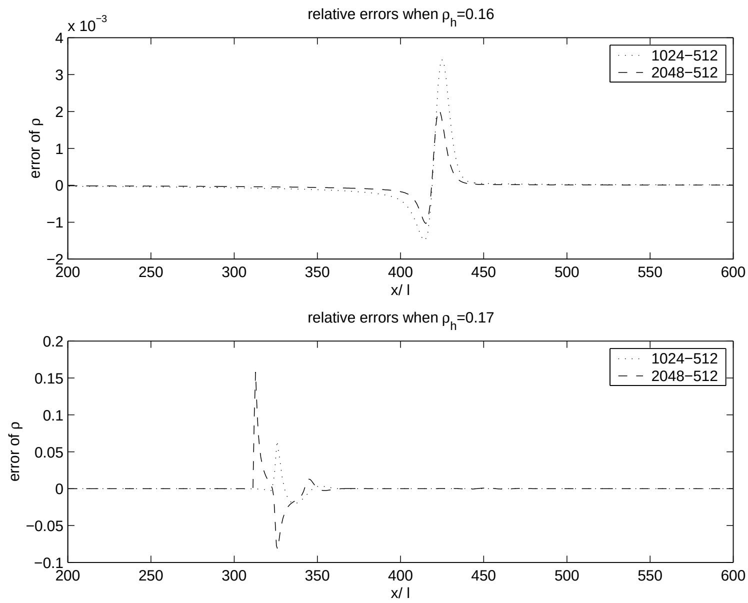

Figure 4.3: Stability and instability for (4.93,4.94) with Periodic boundary condition

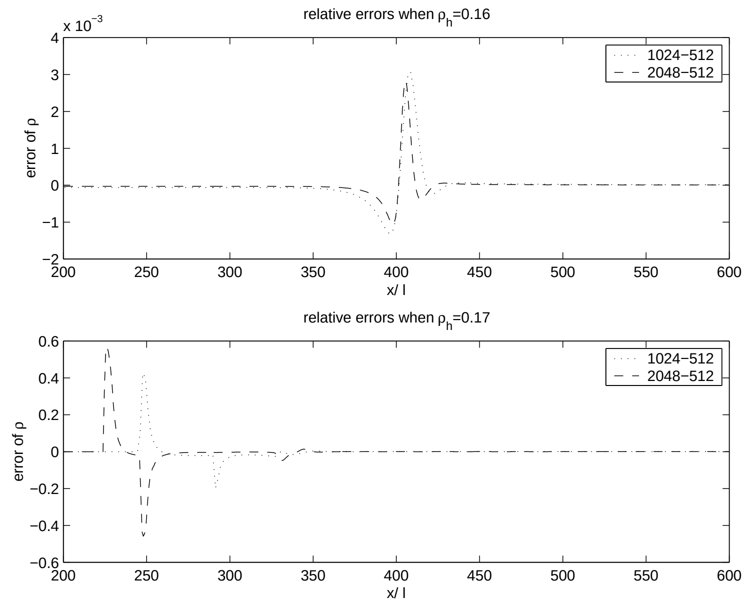

Figure 4.4: Stability and instability for (4.93,4.94) with Neumann boundary condition

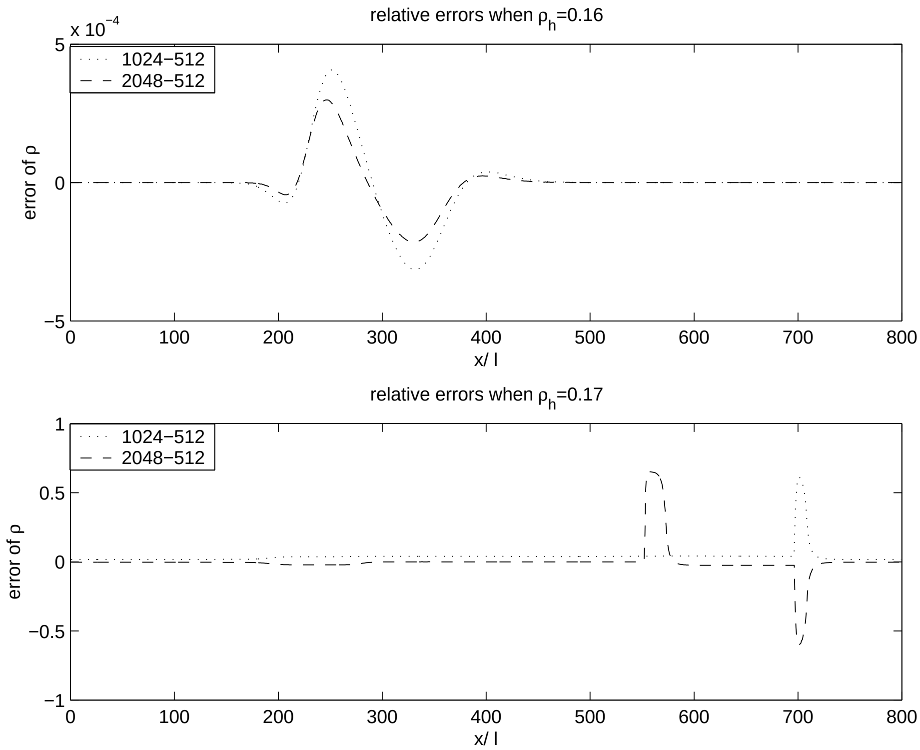

Figure 4.5: Stability and instability for (4.95,4.96) with Periodic boundary condition

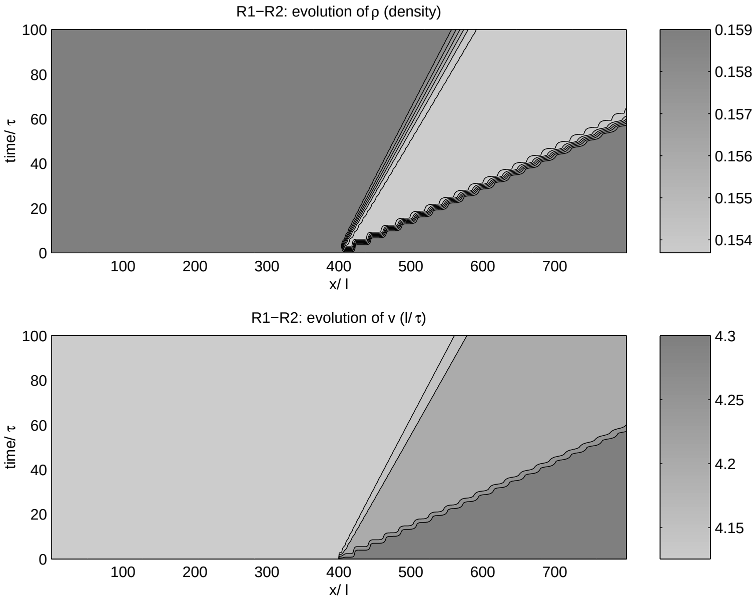

Figure 4.6: The R1-R2 wave solutions to the Riemann problem

ble when $\rho_h = 0.17$. We don't test the PW model for the local perturbation with Neumann boundary conditions, since we expect the same stability property.

According to the numerical tests, the system is stable when $\max \rho(x, 0) \leq 0.18$ and unstable when $\max \rho(x, 0) \geq 0.19$, which is consistent with the theoretical prediction.

4.4.2 The Riemann problem and steady-state solutions

In this subsections, we solve the PW model with four well-selected initial conditions so that we observe second-order waves. The Neumann boundary conditions are used and the number of grids is set as $N = 1024$. We also change the relaxation term to $\frac{f_* - m}{1000\tau}$. The relaxation time 1000τ is long enough for us to watch the second-order waves at $T_0 = 100\tau$, before all 2-waves relax to 1-waves.

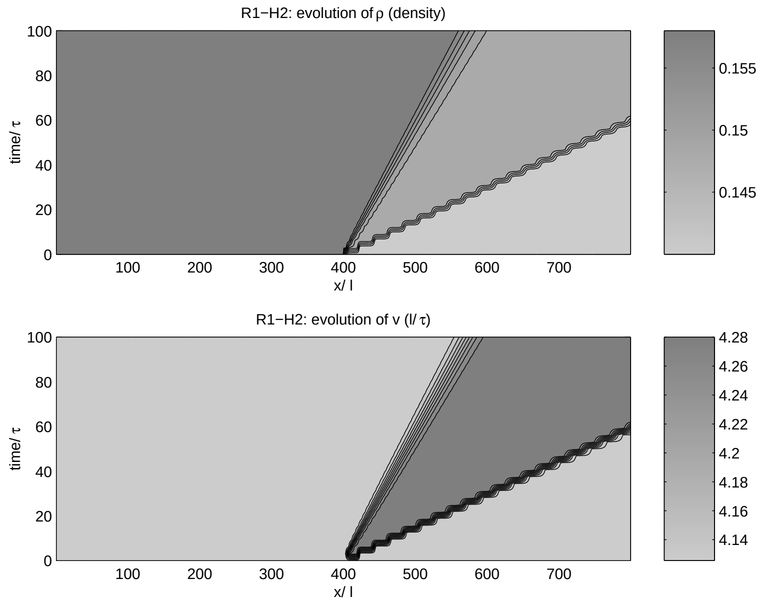

Figure 4.7: The R1-H2 wave solutions to the Riemann problem

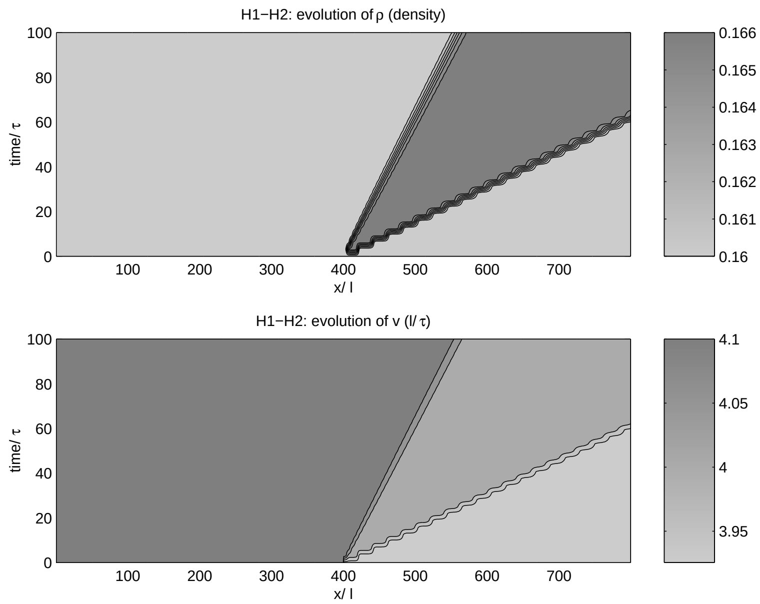

Figure 4.8: The H1-H2 wave solutions to the Riemann problem

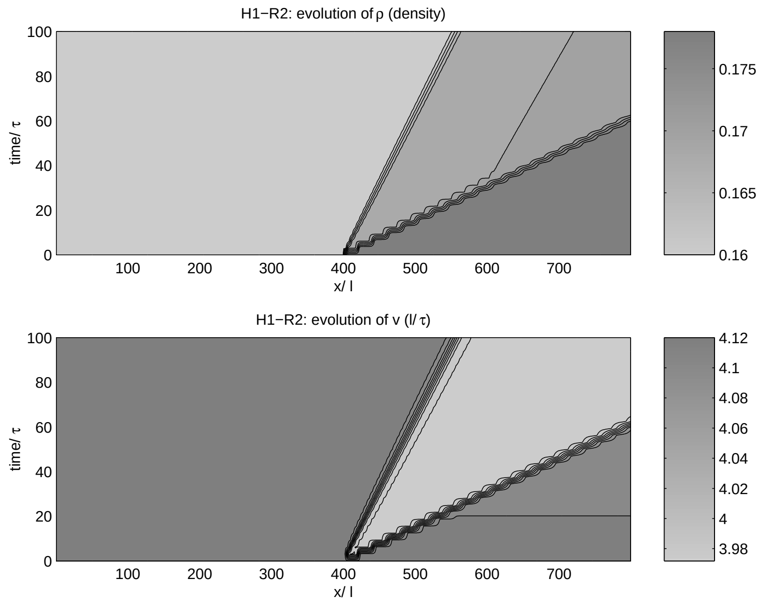

Figure 4.9: The H1-R2 wave solutions to the Riemann problem

1. We use the following jump initial conditions

$$\rho(x,0) = 0.16 \tag{4.97}$$

$$v(x,0) = \begin{cases} v_l = v_*(0.16) & \text{when } x <= 400l \\ v_r = v_*(0.16) + 0.2l/\tau & \text{when } x > 400l \end{cases}. \tag{4.98}$$

The solutions to the Riemann problem are a R1-R2 wave, given in **Figure** 4.6.

2. We use the following jump initial conditions

$$\rho(x,0) = \begin{cases} \rho_l = 0.16 & \text{when } x <= 400l \\ \rho_r = 0.16 - 0.02 & \text{when } x > 400l \end{cases} \tag{4.99}$$

$$v(x,0) = v_*(0.16). \tag{4.100}$$

The wave solutions to the Riemann problem of the PW model are a R1-H2 wave, given in **Figure** 4.7.

3. We use the following jump initial conditions

$$\rho(x,0) = 0.16 \quad (4.101)$$

$$v(x,0) = \begin{cases} v_l = v_*(0.16) & \text{when } x <= 400l \\ v_r = v_*(0.16) - 0.2l/\tau & \text{when } x > 400l \end{cases}. \quad (4.102)$$

   The wave solutions are a H1-H2 wave, given in **Figure** 4.8.

4. We use the following jump initial conditions

$$\rho(x,0) = \begin{cases} \rho_l = 0.16 & \text{when } x <= 400l \\ \rho_r = 0.16 + 0.02 & \text{when } x > 400l \end{cases} \quad (4.103)$$

$$v(x,0) = v_*(0.16). \quad (4.104)$$

   The wave solutions are a H1-R2 wave, given in **Figure** 4.9.

The solutions above show four different type of second-order waves, which consist of two basic waves. However, 2-waves relax to 1-waves if the relaxation time is shorter or the observing time is longer. A 2-shock wave relaxes to a 1-rarefaction wave; and a 2-rarefaction wave relaxes to a 1-shock wave, due to the effect of the source term. In next part, we show how the 2-waves relax to 1-waves and how the free regions and cluster regions form. We set relaxation time as 10τ, and observe the solutions until $T_0 = 100\tau$.

1. With the initial conditions (4.97, 4.98), we get the solutions shown in **Figure** 4.10. At around 5τ a downstream 1-shock forms when the traffic conditions relax to the equilibrium state, i.e., $v = v_*(0.16)$. After that traffic flow forms a free region with lower density and higher travel speed. The free region travels in the speed of λ_*. However the free region will disappear as the R1-H1 wave propagates, and finally the traffic flow will become uniform.

2. With the initial conditions (4.99, 4.100), we get the solutions shown in **Figure** 4.11. A new 1-rarefaction wave forms when the H2-wave disappears. As these

two rarefaction waves propagate, the traffic conditions will become uniform.

3. With the initial conditions (4.101, 4.102), we get the solutions shown in **Figure** 4.12. At around 5τ, the 2-shock wave disappears and a 1-rarefaction wave forms. After that a cluster, with higher density and lower travel speed, travels with at the speed of λ_*. However, the traffic conditions will become uniform as the H1-R1 wave propagates.

4. With the initial conditions (4.103, 4.104), we get the solutions shown in **Figure** 4.13. As long as the 2-rarefaction disappears, a new 1-shock is formed. After that, both shock waves travel in the speed of $\lambda_*(0.16) = 2.12l/\tau$.

In the remaining part of this subsection we consider the steady-state solutions of the system after a long time $T_0 = 1600\tau$ with the relaxation time τ .

1. Using the initial conditions (4.93,4.94) with $\rho_h = 0.16$ and periodic boundary conditions, we get the solutions shown in **Figure** 4.14. The figure shows that an upstream shock wave and a downstream rarefaction wave form. After that, the traffic conditions become more and more uniform.

2. Using the initial conditions (4.95,4.96) with $\rho_h = 0.16$ and periodic boundary conditions, we have the solutions shown in **Figure** 4.15. The solutions show that the traffic conditions get more and more uniform, quicker than the case shown in **Figure** 4.14.

4.4.3 General solutions and convergence rates

In this subsection, different numerical methods for the PW model are discussed with the initial conditions (4.93,4.94) ($\rho_h = 0.16$). Using Neumann boundary conditions, we solve the PW model until $T_0 = 400\tau$. With the number of grids as 64, 128, 256, 512 or 1024, we carry out 5 separate computations. For 1024 grids, we plot the contour

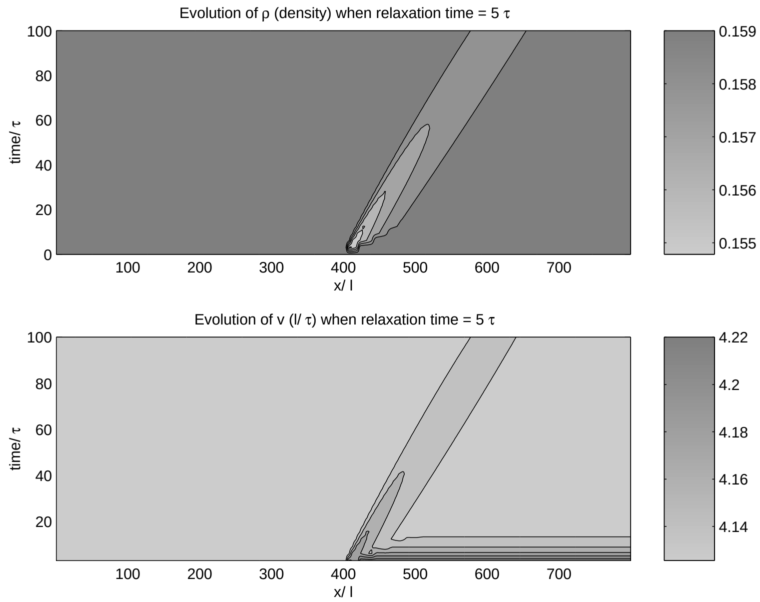

Figure 4.10: Formation of a free region

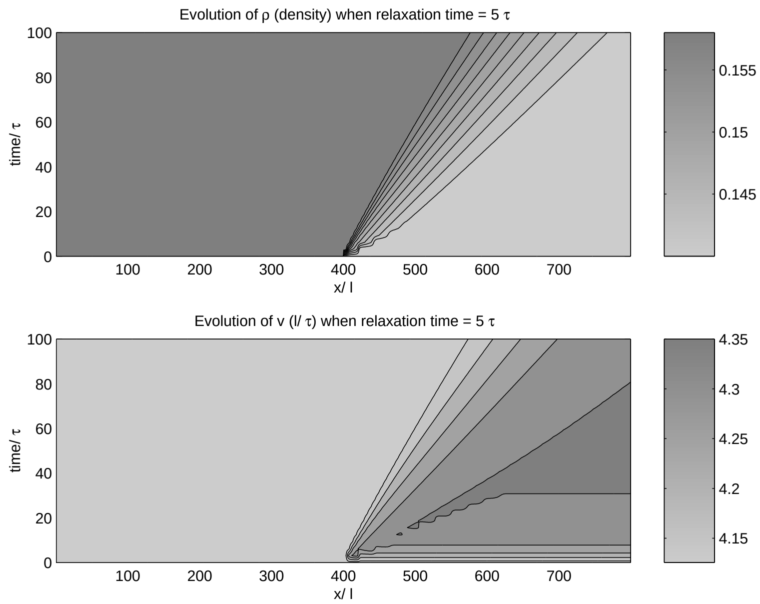

Figure 4.11: Formation of two 1-rarefaction waves

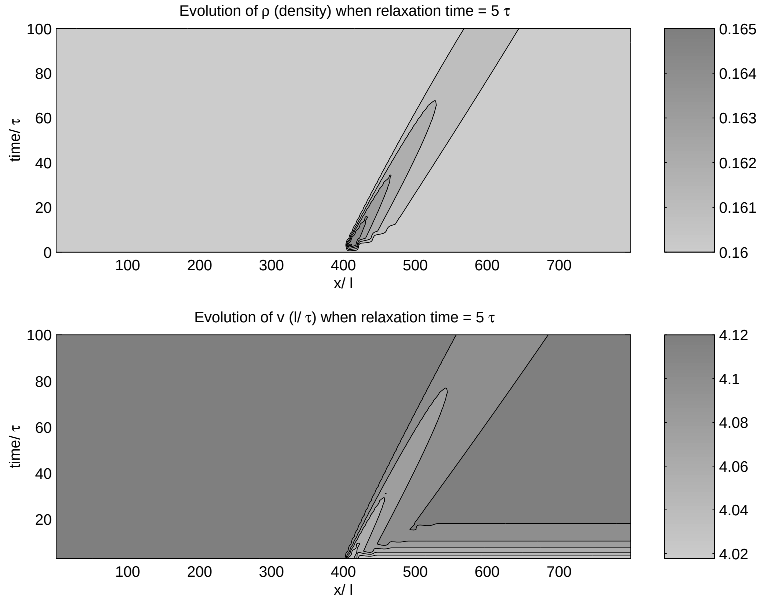

Figure 4.12: Formation of a cluster

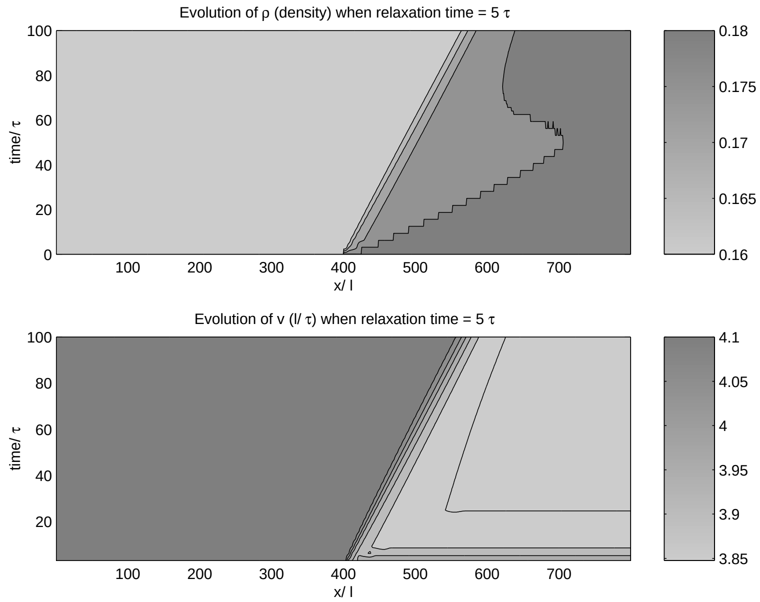

Figure 4.13: Formation of two 1-shock waves

ρ	128-64	Rate	256-128	Rate	512-256	Rate	1024-512
L^1	7.36e-04	9.72e-01	3.75e-04	9.95e-01	1.88e-04	9.69e-01	9.62e-05
L^2	9.38e-04	6.65e-01	5.92e-04	6.81e-01	3.69e-04	6.74e-01	2.31e-04
L^∞	3.07e-03	4.02e-02	2.99e-03	1.79e-01	2.64e-03	3.27e-01	2.10e-03
v	128-64	Rate	256-128	Rate	512-256	Rate	1024-512
L^1	9.68e-03	9.67e-01	4.95e-03	9.99e-01	2.48e-03	9.59e-01	1.27e-03
L^2	1.27e-02	6.43e-01	8.14e-03	6.63e-01	5.14e-03	6.56e-01	3.27e-03
L^∞	4.41e-02	4.81e-02	4.27e-02	1.76e-01	3.78e-02	3.15e-01	3.04e-02

Table 4.1: Convergence rates for the first-order Godunov's method

of ρ and v on the $x - t$ phase plane as well as their solutions at selected times. We also compute the convergence rates based on solutions with different number of grids. The convergence rate is defined in (3.73 – 3.74).

The first-order Godunov's method gives the solutions shown in **Figure** 4.16 and **Figure** 4.17. The relative errors and convergence rates are given by **Table** 4.1. From the table, we can see that for L^1 norm the method is almost of first order, but for L^2 or L^∞ norms, the rate of convergence is lower.

The quasi-steady wave-propagation algorithm by LeVeque (1998a, 1998b) gives the solutions shown in **Figure** 4.18 and **Figure** 4.19 for 1024 grids. The relative errors and convergence rates are given in **Table** 4.2. This scheme de-estimate the effects of the source term, since the convergence rates of ρ and v are totally different.

The fractional step splitting method gives solutions of the PW model shown in **Figure** 4.20 and **Figure** 4.21 for 1024 grids. The relative errors and convergence rates are given in **Table** 4.3. We find that the fractional step splitting method is not so stable as the first-order method, since convergence rates have big oscillations.

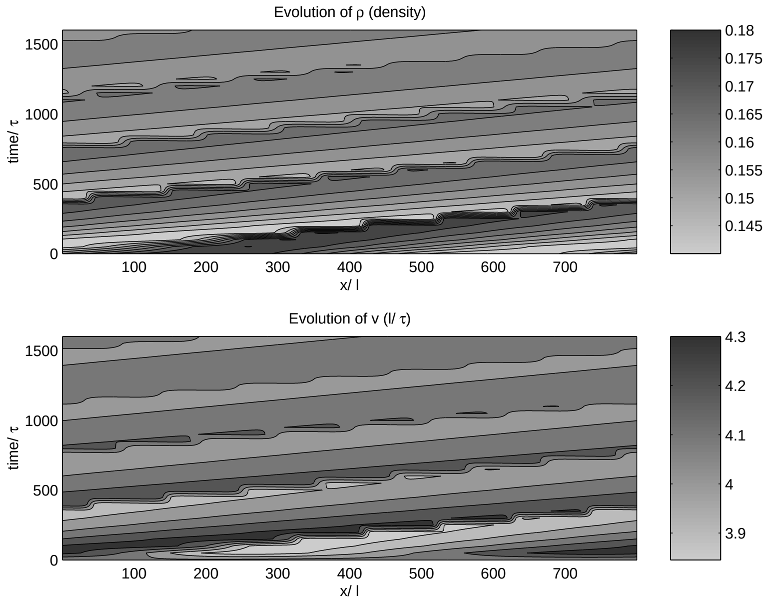

Figure 4.14: Solution for (4.93,4.94) till 1600τ

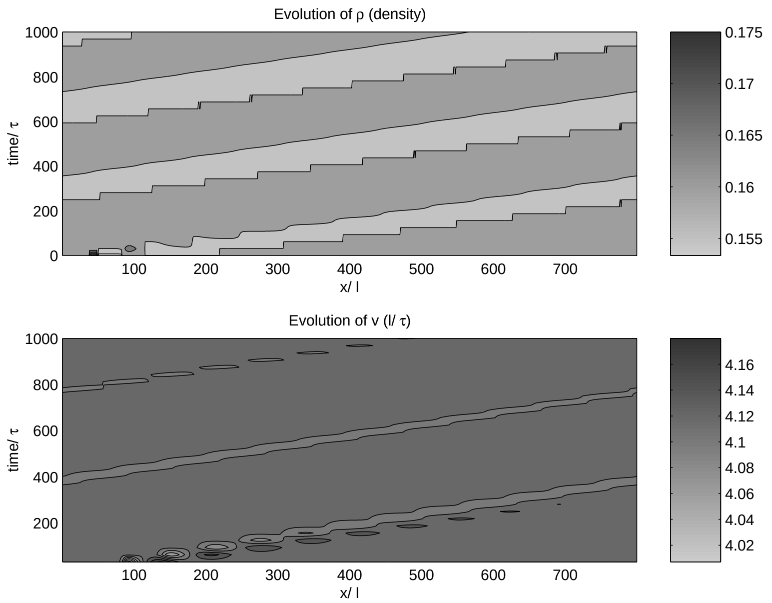

Figure 4.15: Solution for (4.95,4.96) till 1000τ

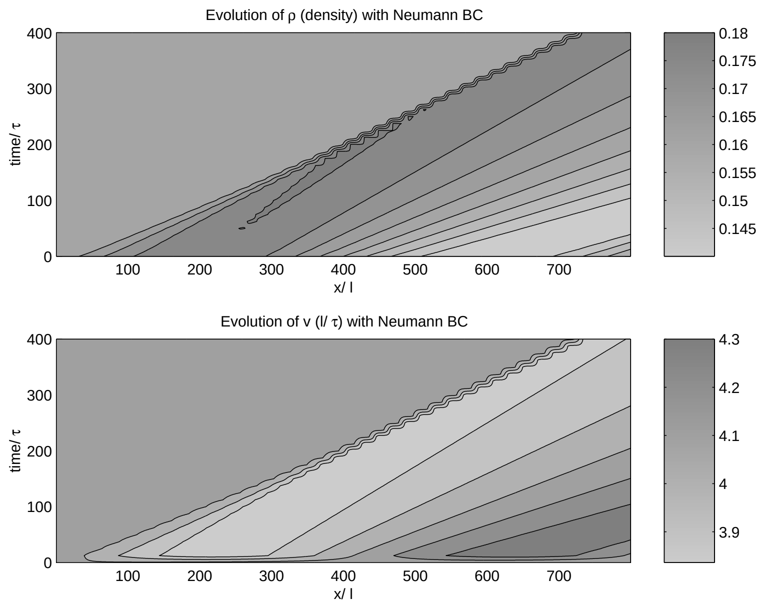

Figure 4.16: Solutions by a first-order Godunov's method for 1024 grids

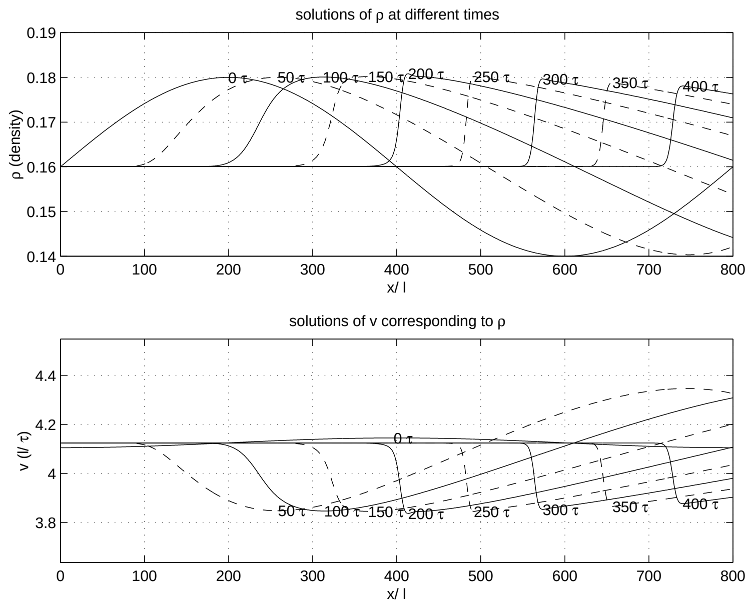

Figure 4.17: Solutions from **Figure** 4.16 at selected times

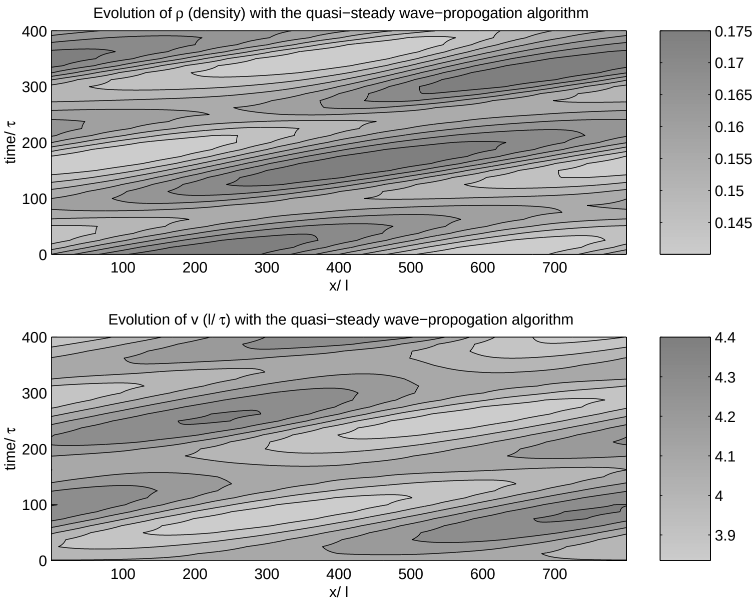

Figure 4.18: Solutions by LeVeque's method for 1024 grids

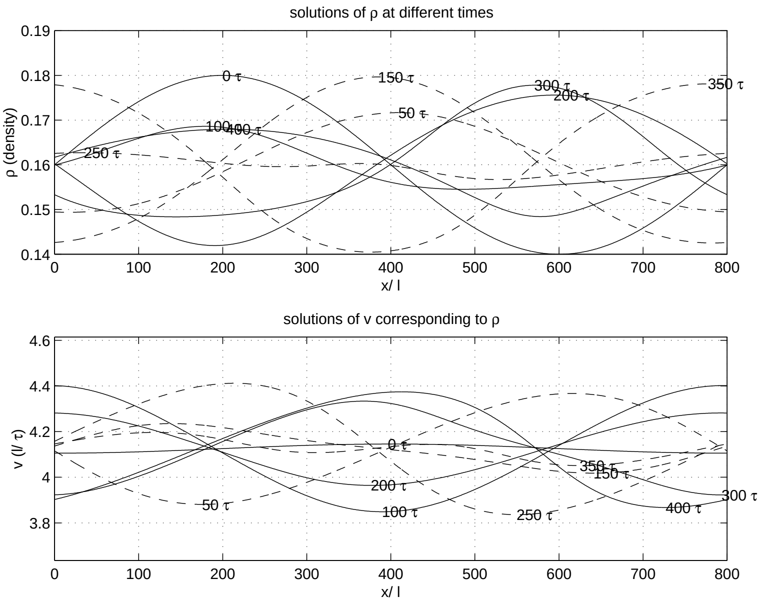

Figure 4.19: Solutions from **Figure** 4.18 at selected times

ρ	256-128	Rate	512-256	Rate	1024-512
L^1	2.09e-02	5.10e-01	1.47e-02	1.16e+00	6.54e-03
L^2	2.28e-02	4.88e-01	1.63e-02	1.14e+00	7.40e-03
L^∞	3.49e-02	5.81e-01	2.33e-02	8.86e-01	1.26e-02
v	256-128	Rate	512-256	Rate	1024-512
L^1	3.42e-02	-1.61e+00	1.05e-01	6.18e-02	1.00e-01
L^2	3.91e-02	-1.58e+00	1.17e-01	5.78e-02	1.12e-01
L^∞	6.96e-02	-1.30e+00	1.71e-01	-1.51e-01	1.90e-01

Table 4.2: Convergence rates for the quasi-steady wave-propagation algorithm

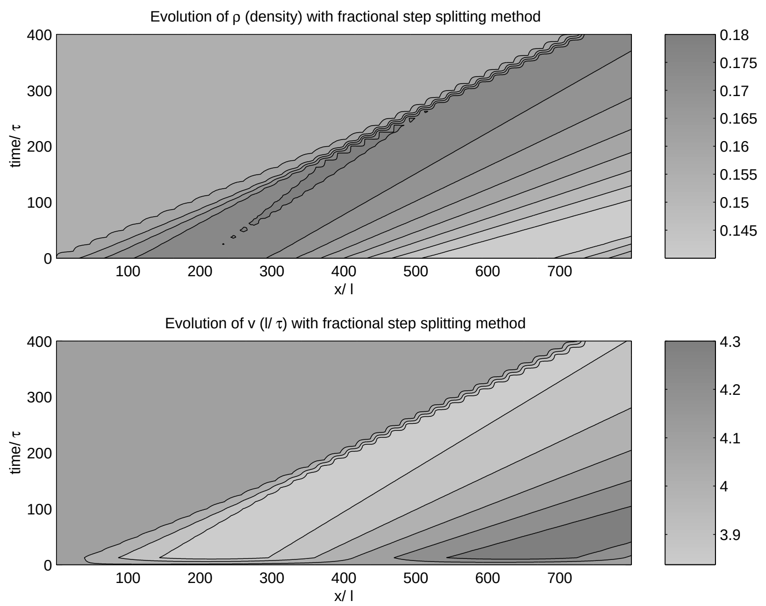

Figure 4.20: Solutions by fractional splitting method for 1024 grids

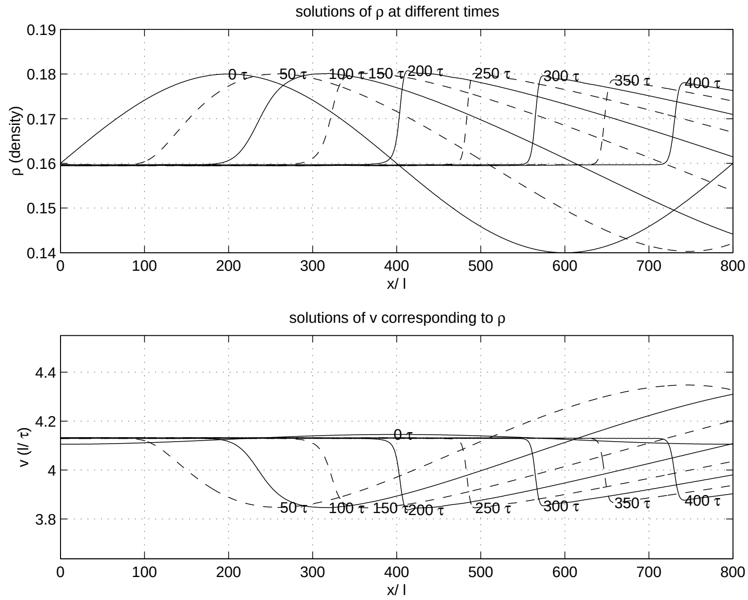

Figure 4.21: Solutions from **Figure** 4.20 at different times

ρ	128-64	Rate	256-128	Rate	512-256	Rate	1024-512
L^1	8.27e-04	9.49e-01	4.28e-04	-5.45e-01	6.25e-04	1.38e+00	2.41e-04
L^2	1.00e-03	7.35e-01	6.01e-04	-2.72e-01	7.26e-04	5.81e-01	4.85e-04
L^∞	2.83e-03	1.95e-01	2.47e-03	-4.07e-01	3.28e-03	-4.48e-01	4.47e-03
v	128-64	Rate	256-128	Rate	512-256	Rate	1024-512
L^1	1.08e-02	9.46e-01	5.58e-03	-5.01e-01	7.90e-03	1.35e+00	3.11e-03
L^2	1.33e-02	7.14e-01	8.13e-03	-1.92e-01	9.28e-03	4.76e-01	6.67e-03
L^∞	3.86e-02	1.19e-01	3.55e-02	-2.77e-01	4.30e-02	-5.32e-01	6.22e-02

Table 4.3: Convergence rates for the fractional step splitting method

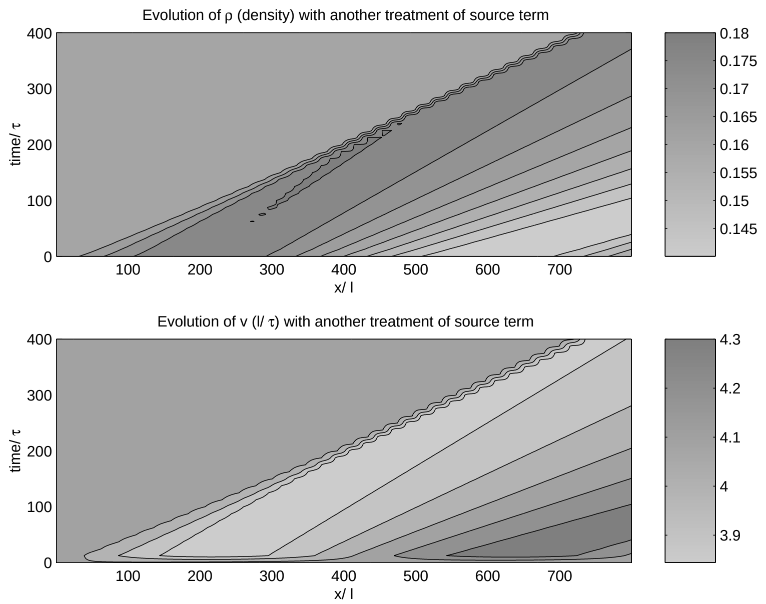

Figure 4.22: Solutions by Pember's method for 1024 grids

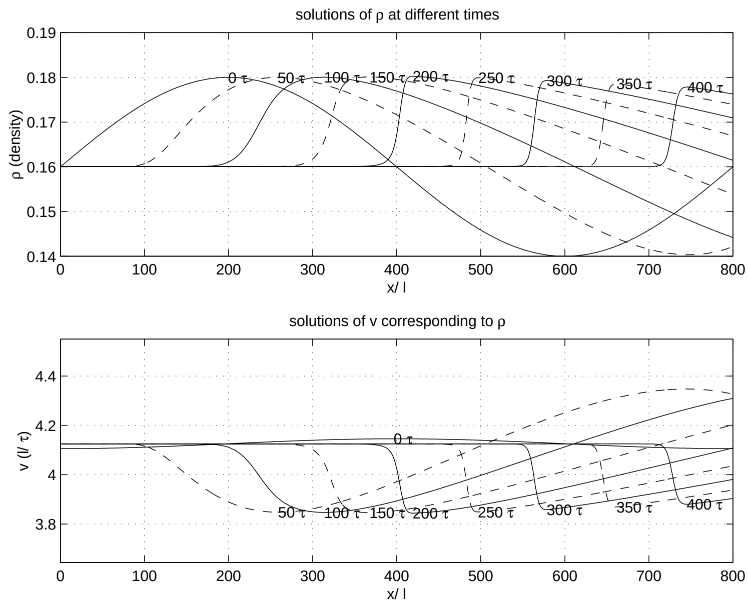

Figure 4.23: Solutions from **Figure** 4.22 at different times

ρ	128-64	Rate	256-128	Rate	512-256	Rate	1024-512
L^1	8.31e-04	7.69e-01	4.88e-04	9.73e-01	2.49e-04	1.02e+00	1.22e-04
L^2	1.07e-03	4.67e-01	7.76e-04	6.39e-01	4.98e-04	6.82e-01	3.10e-04
L^∞	2.94e-03	-4.29e-02	3.03e-03	9.29e-02	2.84e-03	2.85e-01	2.33e-03
v	128-64	Rate	256-128	Rate	512-256	Rate	1024-512
L^1	1.10e-02	7.60e-01	6.50e-03	9.73e-01	3.31e-03	1.02e+00	1.64e-03
L^2	1.46e-02	4.52e-01	1.06e-02	6.33e-01	6.87e-03	6.74e-01	4.30e-03
L^∞	4.09e-02	-4.25e-02	4.21e-02	9.82e-02	3.94e-02	2.78e-01	3.24e-02

Table 4.4: Convergence rates for Pember's method

Pember's method (1993a, 1993b) give the solutions shown in **Figure** 4.22 and **Figure** 4.23 for 1024 grids. The relative errors and convergence rates are given in **Table** 4.4.

In the remaining part of this subsection we consider the second-order Godunov's method. We use $\rho_h = 0.15$ for initial conditions (4.93,4.94), since the second-order method is not stable for $\rho_h = 0.16$. For 1024 grids, we get the solutions shown in **Figure** 4.24 and **Figure** 4.25. The relative errors and convergence rates are given in **Table** 4.5.

Comparing the convergence rates with those for first-order Godunov's method, we see no significant improvement. This is different from the case for Zhang's model. This is a special property of the PW model.

4.4.4 Unstable solutions of the PW model

In this subsection we check the unstable solutions of the PW model. We use the first-order Godunov's method with periodic boundary conditions, and we observe the

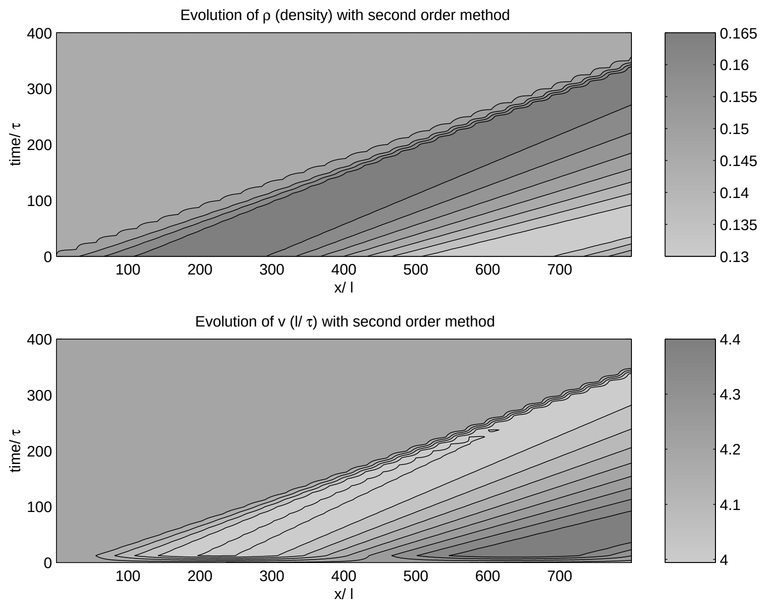

Figure 4.24: Solutions by the second-order Godunov's method for 1024 grids

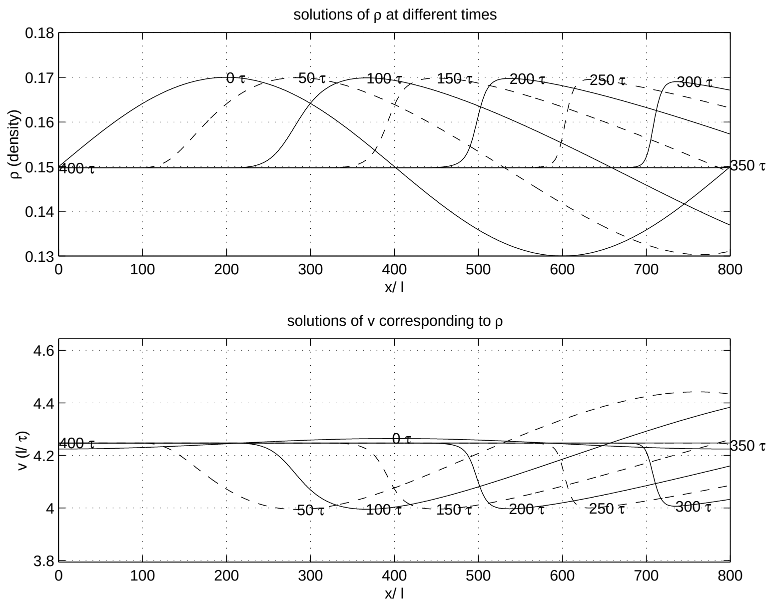

Figure 4.25: Solutions from **Figure** 4.24 at selected times

ρ	128-64	Rate	256-128	Rate	512-256	Rate	1024-512
L^1	5.34e-04	1.29e+00	2.18e-04	1.19e+00	9.55e-05	1.03e+00	4.69e-05
L^2	5.34e-04	1.29e+00	2.18e-04	1.19e+00	9.55e-05	1.03e+00	4.69e-05
L^∞	5.34e-04	1.29e+00	2.18e-04	1.17e+00	9.65e-05	1.01e+00	4.78e-05
v	128-64	Rate	256-128	Rate	512-256	Rate	1024-512
L^1	6.02e-03	1.30e+00	2.45e-03	1.19e+00	1.07e-03	1.03e+00	5.26e-04
L^2	6.02e-03	1.30e+00	2.45e-03	1.19e+00	1.07e-03	1.03e+00	5.26e-04
L^∞	6.02e-03	1.30e+00	2.45e-03	1.18e+00	1.08e-03	1.01e+00	5.36e-04

Table 4.5: Convergence rate for second-order method

solutions at $T_0 = 200\tau$ for different number of grids.

We use the initial conditions (4.93,4.94) with $\rho_h = 0.175$, which is in the unstable region of the PW model. Solutions of the PW model are listed as the following for different number of grids:

1. For 512 grids, solutions are given in **Figure** 4.26 and **Figure** 4.27.
2. For 1024 grids, solutions are given in **Figure** 4.28 and **Figure** 4.29.
3. For 2048 grids, solutions are given in **Figure** 4.30 and **Figure** 4.31.

The figures show that the number and position of spikes are different for different number of grids. This difference is caused by different approximations used by Godunov's method for different number of grids, since the PW model is unstable in the region where the initial conditions are.

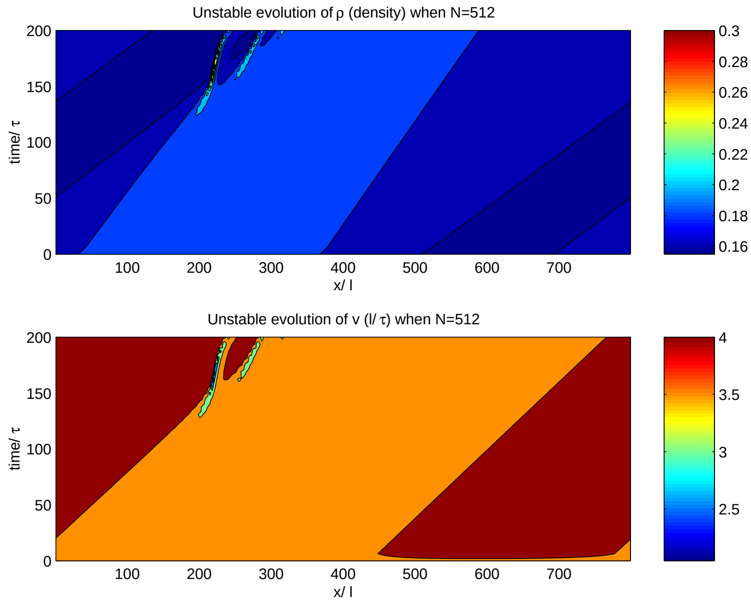

Figure 4.26: Solutions for 512 grids with initial conditions (4.93,4.94)

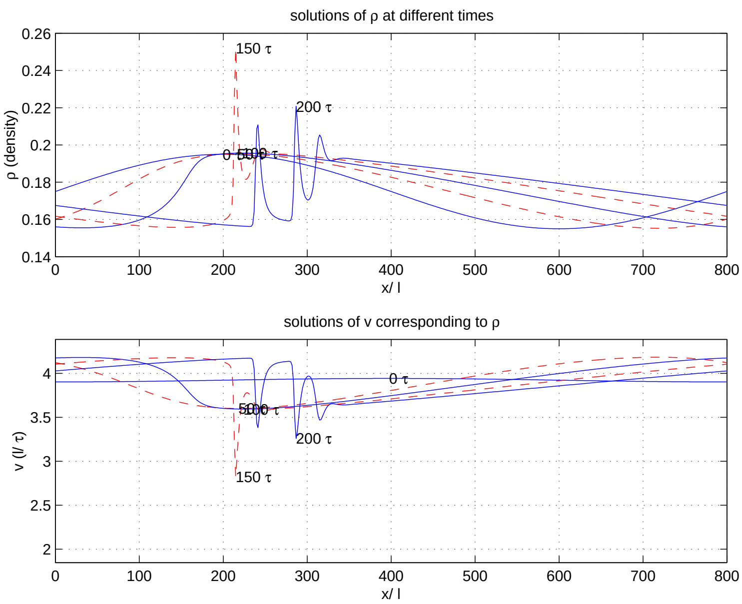

Figure 4.27: Solutions from **Figure** 4.26 at selected times

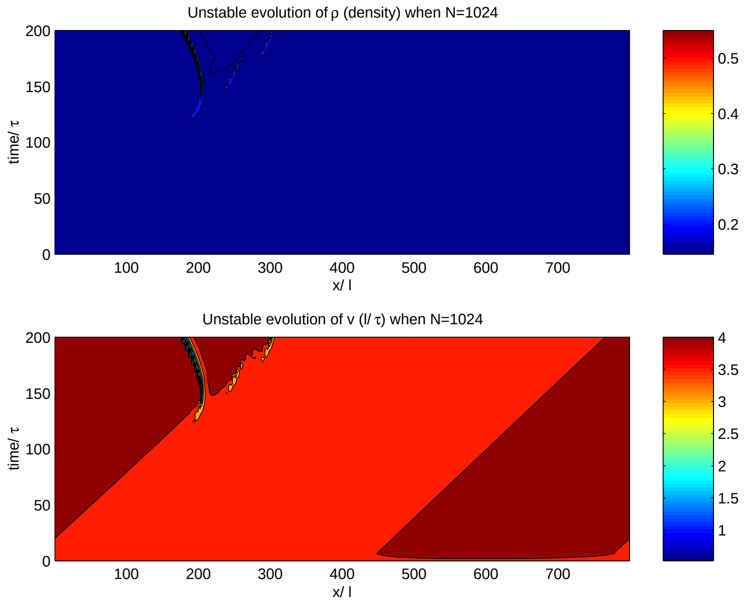

Figure 4.28: Solutions for 1024 grids with initial conditions (4.93,4.94)

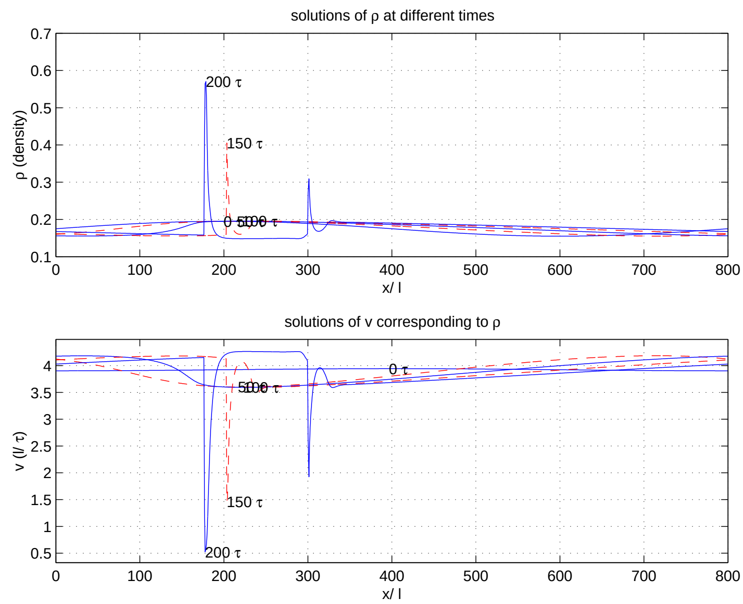

Figure 4.29: Solutions from **Figure** 4.28 at selected times

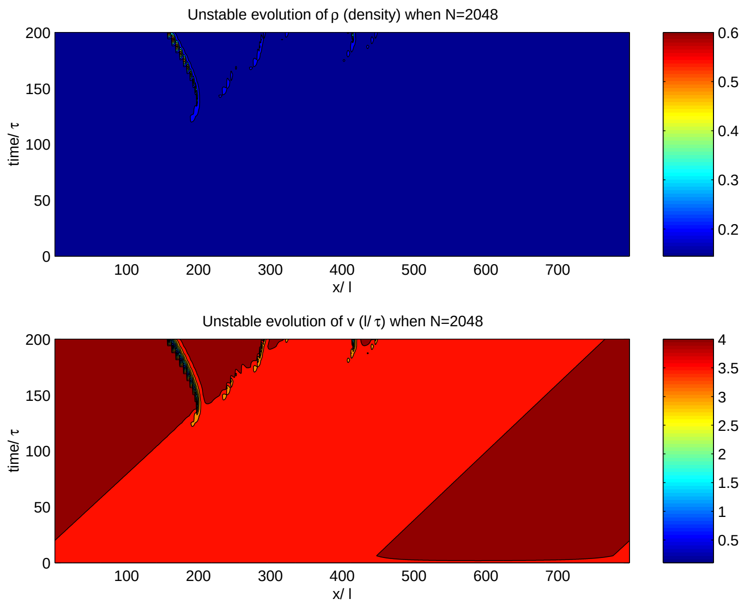

Figure 4.30: Solutions for 2048 grids with initial conditions (4.93,4.94)

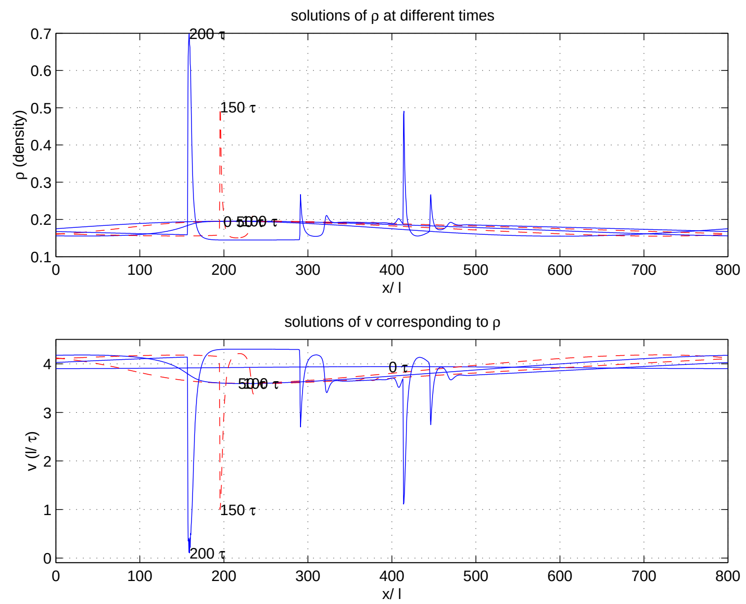

Figure 4.31: Solutions from **Figure** 4.30 at selected times

Chapter 5

The Inhomogeneous LWR Model and Its Numerical Solutions

5.1 Introduction

The LWR model (Lighthill and Whitham, 1955;Richards, 1956) was introduced based on the conservation of traffic flow, and is written as:

$$\frac{\partial}{\partial t}\rho + \frac{\partial}{\partial x} f \quad = \quad 0. \tag{5.1}$$

The LWR model assumes that traffic flow is in equilibrium, or equivalently that travel speed v (unit: mph) is defined as a function of traffic density ρ (unit: vpm) at any location x:

$$v = v_*(x, \rho). \tag{5.2}$$

The function of flow rate $f = \rho v_*(x, \rho)$ (unit: vph) is called a fundamental diagram. For typical equilibrium traffic flows, travel speed is a decreasing function; i.e., $v_{*\rho} < 0$, and traffic flow rate is a concave function; i.e., $f_{\rho\rho} < 0$.

The homogeneous LWR model is for modeling a homogeneous road, where travel speed v_* is uniform with respect to location x. The homogeneous LWR model can thus be written as

$$\rho_t + f(\rho)_x = 0. \tag{5.3}$$

The homogeneous LWR model is a scalar conservation law, and there have been many methods to compute its entropy solutions (Lebacque, 1995). It's well-known that the entropy solutions exist and are unique under the so-called "Lax entropy condition". For computation of these entropy solutions, the Godunov method is most often used.

For a road with inhomogeneity, such as variable number of lanes, curvature and slope, we can formulate the inhomogeneous LWR model as

$$\rho_t + f(a, \rho)_x = 0, \tag{5.4}$$

where $a = a(x)$ is a time-invariant variable. The inhomogeneity factor $a(x)$ gives a profile of a piece of roadway, for example $a(x)$ can be the number of lanes at location x.

The inhomogeneous LWR model has been studied by Daganzo (1994) and Lebacque (1995) and Daganzo (1994). Both of these authors suggested solutions to the inhomogeneous LWR model, and their solutions are consitent. However, these studies only presented empirical solutions without rigorous proof.

The difficulty of dealing with the inhomogeneous LWR model is due to the extra variable $a(x)$. Here, by introducing $a(x)$ as an additional conservation law, we consider the inhomogeneous LWR model as a resonant nonlinear system, which has been discussed in (Isaacson & Temple, 1992; Lin et al., 1995). In this chapter, we follow the procedures provided in those researches to study the inhomogeneous LWR model.

This chapter is organized as follows. In section 2, we formulate the inhomogeneous traffic model as a resonant nonlinear system, and its properties are discussed. In section 3, we solve Riemann problem for the inhomogeneous LWR model. In section

4 we present the numerical methods for this model. We conclude the discussions of this chapter in section 5.

5.2 The Properties of the inhomogeneous LWR model

To apply the results for hyperbolic systems of conservation laws, we express the inhomogeneity factor $a(x)$ as an additional conservation law, i.e., $a_t = 0$. Hence, we can write the inhomogeneous LWR model as

$$U_t + F(U)_x = 0, \tag{5.5}$$

where $U = (a, \rho), F(U) = (0, f(a, \rho)), x \in R, t \geq 0$. In this chapter we consider one type of inhomogeneity – variable number of lanes. The fundamental diagram is thus written as $f(a, \rho) = \rho v_*(\frac{\rho}{a})$, given that all the lanes are of the same condition.

The inhomogeneous LWR model (5.5) can be linearized as

$$U_t + DF(U)U_x = 0, \tag{5.6}$$

where the differential $DF(U)$ of the flux vector $F(U)$ is

$$DF = \begin{bmatrix} 0 & 0 \\ -\frac{\rho^2}{a^2}v_*'(\frac{\rho}{a}) & v_*(\frac{\rho}{a}) + \frac{\rho}{a}v_*'(\frac{\rho}{a}) \end{bmatrix}. \tag{5.7}$$

The two eigenvalues for DF are

$$\lambda_0 = 0 \qquad \lambda_1 = v_*(\frac{\rho}{a}) + \frac{\rho}{a}v_*'(\frac{\rho}{a}). \tag{5.8}$$

The corresponding right eigenvectors are

$$\mathbf{R}_0 = \begin{bmatrix} v_*(\frac{\rho}{a}) + \frac{\rho}{a}v_*'(\frac{\rho}{a}) \\ (\frac{\rho}{a})^2 v_*'(\frac{\rho}{a}) \end{bmatrix} \qquad \mathbf{R}_1 = \begin{bmatrix} 0 \\ 1 \end{bmatrix},$$

and the left eigenvector of $\partial f/\partial \rho$ as $\mathbf{l}_1 = 1$. The system (5.5) is a non-strictly hyperbolic system, since λ_1 may be equal to $\lambda_0 = 0$.

We consider a traffic state $U_* = (a_*, \rho_*)$ as critical if

$$\lambda_1(U_*) = 0; \tag{5.9}$$

i.e., at critical states, the two wave speeds are the same and system (5.5) is singular. For a critical traffic state U_* we also have

$$\frac{\partial}{\partial \rho}\lambda_1(U_*) \quad = \quad f_{\rho\rho} < 0, \tag{5.10}$$

and

$$\frac{\partial}{\partial a} f(U_*) \quad = \quad -(\frac{\rho}{a})^2 v_*'(\frac{\rho}{a})|_{U_*} = \frac{\rho}{a} v_*(\frac{\rho}{a})|_{U_*} > 0. \tag{5.11}$$

A consequence of properties (5.10) and (5.11) is that the linearized system (5.6) at U_* has the following normal form

$$\begin{bmatrix} \delta a \\ \delta \rho \end{bmatrix}_t + \begin{bmatrix} 0 & 0 \\ 1 & 0 \end{bmatrix} \begin{bmatrix} \delta a \\ \delta \rho \end{bmatrix}_x \quad = \quad 0. \tag{5.12}$$

The system (5.12) has the solution $\delta\rho(x,t) = \delta a'(x)t + c$, and the solution goes to infinity as t goes to infinity. Therefore (5.12) is a linear resonant system, and the original inhomogeneous LWR model (5.5) is a nonlinear resonant system.

For (5.5), the smooth curve Γ in U-space formed by all critical states U_* are named a transition curve. Therefore Γ is defined as

$$\Gamma \quad = \quad \{U | \lambda_1(U) = 0\}.$$

Since $\lambda_1(U) = v_*(\frac{\rho}{a}) + \frac{\rho}{a} v_*'(\frac{\rho}{a})$, we obtain

$$\Gamma \quad = \quad \left\{(a,\rho) | \frac{\rho}{a} = \alpha, \text{ where } \alpha \text{ uniquely solves } v_*(\alpha) + \alpha v_*'(\alpha) = 0\right\}; \tag{5.13}$$

i.e., the transition curve for (5.5) is a straight line passing through the origin in U-space. In (5.13), α is unique since $f(a,\rho)$ is concave in ρ.

The entropy solutions to a nonlinear resonant system are different from those to a strict hyperbolic system of conservation laws. Isaacson & Temple (1992) proved

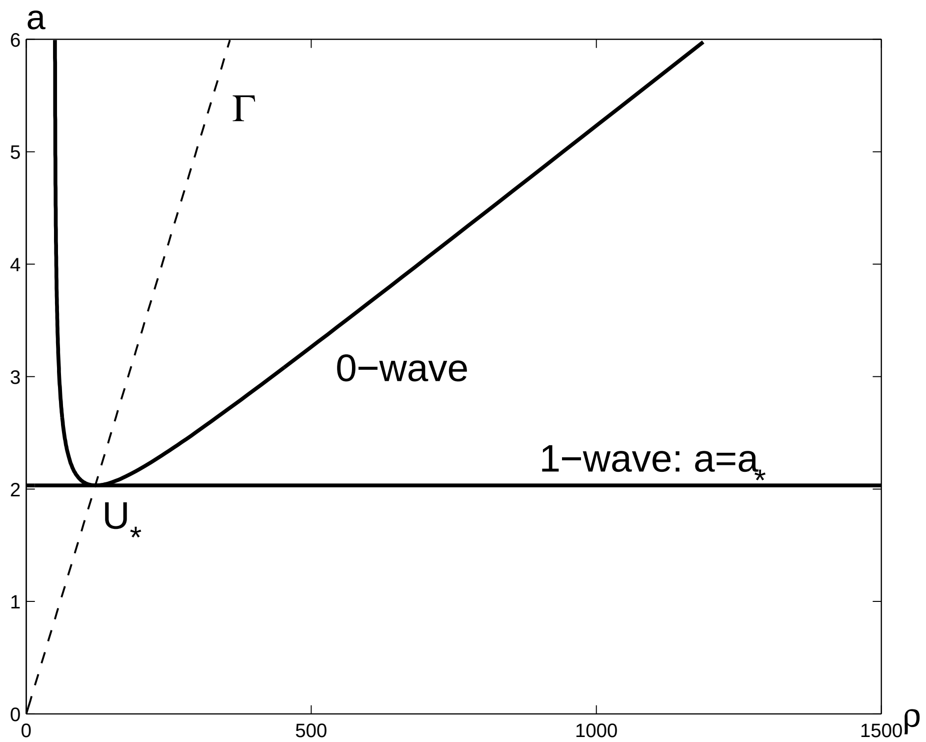

Figure 5.1: Integral curves

that solutions to the Riemann problem for system (5.5) exist and are unique with the conditions (5.9)-(5.11). Lin et al. (1995) also presented solutions to a scalar nonlinear resonant system, which is similar to our system (5.5) except that f is convex. In the next section we apply those results to solve the Riemann problem for the inhomogeneous LWR model.

5.3 Solutions to the Riemann problem

In this section we study the wave solutions to the Riemann problem for (5.5) with the following jump initial conditions

$$U(x,t=0) \quad = \quad \begin{cases} U_L & \text{if } x<0 \\ U_R & \text{if } x>0 \end{cases}, \tag{5.14}$$

where the initial values of U_L, U_R are constant. For computational purpose, we are interested in the average flux at the boundary $x=0$ over a time interval Δt, which is denoted by f_0^*; i.e., we want to find

$$f_0^* \quad = \quad \frac{1}{\Delta t}\int_0^{\Delta t} f(U(x=0,t))\mathrm{dt}. \tag{5.15}$$

The inhomogeneous LWR model (5.5) has two families of basic wave solutions associated to the two eigenvalues. The solutions whose wave speed is λ_0 are in the 0-family, and the waves are called 0-waves. Similarly the solutions whose wave speed is λ_1 are in the 1-family, and the waves are called 1-waves. In U-space, the wave curves for (5.5) are the integral curves of the right eigenvectors $\mathbf{R}_0$ and $\mathbf{R}_1$. Hence the 0-wave curves are given by $f(U)$=const, and the 1-wave curves are given by $a=\bar{a}$, where $\bar{a}$ is constant. The 0-wave is also called a standing wave since its wave speed is always 0. The 1-wave solutions are determined by the solutions of the scalar conservation law $\rho_t + f(\bar{a},\rho)_x = 0$. A 0-wave curve, a 1-wave curve passing a critical state U_* and the transition curve Γ are shown in **Figure** 5.1, where a is set as the vertical axis and ρ is set as the horizontal axis.

As shown in **Figure** 5.1, the 0-wave curve is convex, and the 1-wave curve is tangent to the 0-wave curve at the critical state U_*. The transition curve Γ intersects the 0-wave and 1-wave curves transversely at U_*, and there is only one critical state on one 0-wave or 1-wave curve. For any point U, there is only one 0-wave curve and only one 1-wave curve passing it. In **Figure** 5.1, the states left to the transition

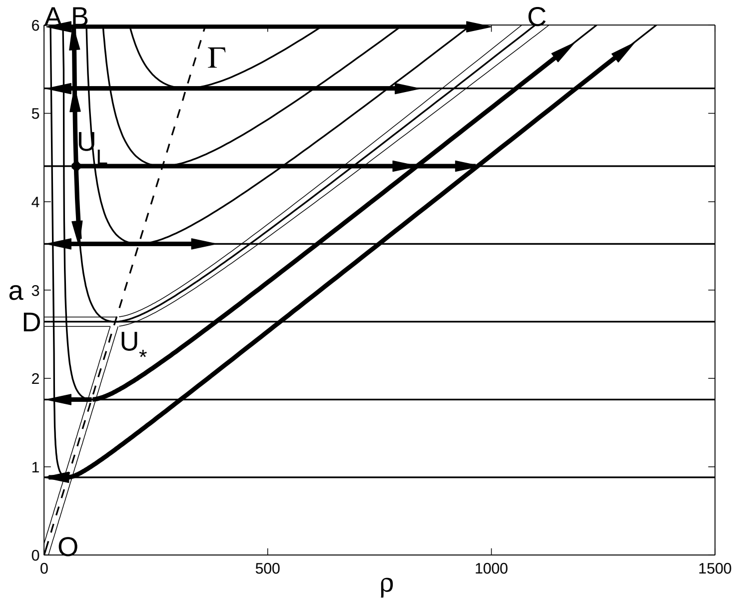

Figure 5.2: The Riemann problem for U_L left of Γ

curve are undercritical since $\rho/a < \alpha$; and the states right to the transition curve are overcritical since $\rho/a > \alpha$.

The wave solutions to the Riemann problem for (5.5) are combinations of basic 0-waves and 1-waves. If we order the waves with respect to space x at any time t, all the waves must satisfy Lax's entropy condition; i.e., the waves from left (upstream) to right (downstream) should increase their wave speeds so that they don't cross each other. This condition is imposed on all hyperbolic systems of conservation laws. For a nonlinear resonant system (5.5), an additional condition has to be imposed; i.e., as long as the standing wave is not interrupted by a shock-wave, its associated density must vary continuously. To guarantee this, the following entropy condition is required:

$$\text{The standing wave can NOT cross the transition curve } \Gamma. \tag{5.16}$$

With the two entropy conditions, the solutions to the inhomogeneous LWR model

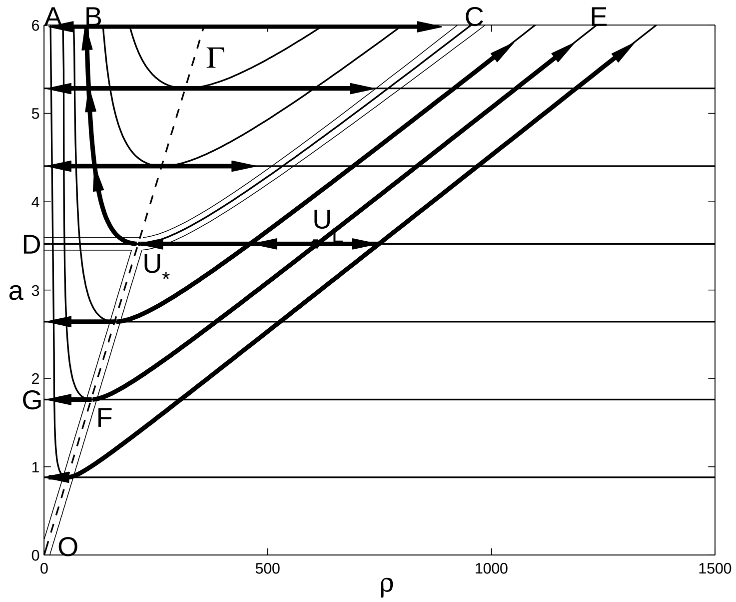

Figure 5.3: The Riemann problem for U_L right of Γ

exist and are unique. The wave solutions for undercritical left state U_L is shown in **Figure** 5.2, and those for overcritical left state U_L is shown in **Figure** 5.3.

In the remaining part of this section, we discuss wave solutions to the Riemann problem for (5.5), present the formula for the boundary flux f_0^* related to each type of solutions, summarize our results and compare them with those existing in literature.

5.3.1 Solutions of the boundary fluxes

When $U_L = (a_L, \rho_L)$ is undercritical; i.e., $\rho_L/a_L < \alpha$, where α is defined in (5.13), we denote the special critical point on standing wave passing U_L as U_*. Thus, as shown in **Figure** 5.2, the U-space is partitioned into three regions by DU_*, OU_* and U_*C, where $DU_* = \{(a,\rho)|a = a_*, \rho < \rho_*\}$, $OU_* = \Gamma \cap \{0 \leq \rho \leq \rho_*\}$ and $U_*C = \{(a,\rho)|f(a,\rho) = f(U_L), \rho > \rho_*\}$. Related to different positions of the right state U_R in the U-space, the Riemann problem for (5.5) with initial conditions (5.14)